



Validation of Nuclear Data for Fusion Applications Using the Quasi-Differential Neutron Scattering Experimental Method

Gregory Siemers & Yaron Danon

To cite this article: Gregory Siemers & Yaron Danon (20 Nov 2025): Validation of Nuclear Data for Fusion Applications Using the Quasi-Differential Neutron Scattering Experimental Method, Fusion Science and Technology, DOI: [10.1080/15361055.2025.2525026](https://doi.org/10.1080/15361055.2025.2525026)

To link to this article: <https://doi.org/10.1080/15361055.2025.2525026>



Published online: 20 Nov 2025.



Submit your article to this journal [↗](#)



View related articles [↗](#)



View Crossmark data [↗](#)



Validation of Nuclear Data for Fusion Applications Using the Quasi-Differential Neutron Scattering Experimental Method

Gregory Siemers¹ and Yaron Danon^{1*}

Rensselaer Polytechnic Institute, Gaerttner LINAC Center, 3021 Tibbits Avenue, Troy, New York 12180

Received December 31, 2024

Accepted for Publication June 19, 2025

Abstract — Neutronics calculations of fusion systems require accurate neutron transport simulations to predict quantities such as shielding effectiveness, material damage and transmutation, and reaction rates. Evaluated nuclear data from the U.S. Evaluated Nuclear Data Library (ENDF), the Joint Evaluated Fission and Fusion File (JEFF), or the Fusion Evaluated Nuclear Data Library (FENDL) are frequently used for these calculations. Therefore, the results from these calculations are highly dependent on the accuracy of the cross sections and angular distributions provided in these evaluated nuclear data libraries. The quasi-differential neutron scattering method was developed to validate the accuracy of evaluated cross sections and angular distributions. These measurements are particularly well suited to validate nuclear data pertaining to nuclear fusion applications. The incident neutron energy region of the measurement, 0.5 to 20 MeV, corresponds with the neutron energy range most relevant to fusion systems where neutron scattering reactions dominate.

Modeling neutron scattering reactions accurately is important since neutrons will only have a few interactions before being absorbed or leaking from a system. In quasi-differential neutron scattering experiments, a white pulsed neutron beam is scattered from a thick sample and neutrons are detected by an array of detectors surrounding the sample. The experimental data are then compared with detailed radiation transport simulations using multiple evaluated nuclear data sets. This comparison provides information about the accuracy of these evaluated data for the sample of interest. The advantage of such a method is the high sensitivity to the nuclear data of the measured sample material with minimal interference from other materials. This method has been successfully utilized to obtain nuclear reaction data of several materials that are important to nuclear fission reactors and criticality safety applications, such as Be, Pb, Fe, Ta, Mo, ²³⁸U, Zr, and F. Moreover, data from these measurements informed certain evaluations in the ENDF/B-VIII.0 and ENDF/B-VIII.1 nuclear data libraries. We propose that quasi-differential neutron scattering will be of great value for the validation of fusion-related materials, such as Si, W, Li, Ti, Nb, and O, and that additional measurements are needed for more materials of interest.

Keywords — Nuclear data, validation, neutron scattering, nuclear fusion.

Note — Some figures may be in color only in the electronic version.

I. INTRODUCTION

Neutron transport methods for fission and fusion systems are used for to determine the neutron flux in the system and other related quantities. The outgoing neutron energy range of interest for nuclear fission and

nuclear fusion systems is different, with neutrons produced in a deuterium-tritium (DT) fusion system beginning at 14 MeV while fission neutrons are created with an average energy of about 2 MeV. Thus, in a DT fusion system, the neutron flux will extend up to 14 MeV, but its resultant energy distribution and magnitude will be determined by subsequent interactions of these 14-MeV neutrons with the device materials.

*E-mail: danony@rpi.edu

Correctly modeling this neutron flux is of utmost importance since all reaction rates, along with isotope and particle production, within the system are directly proportional to it. Unknown errors in the modeled neutron flux of a fusion system from poor nuclear data can lead to the incorrect modeling of several quantities such as:

1. The neutron flux in the breeder and multiplier, leading to incorrect tritium production and/or neutron multiplication.
2. Neutron flux reentering plasma from first wall, blanket, shielding, and structural materials.^[1]
3. Charged particle production, such as helium from inaccurate (n,α) data in potentially sensitive areas of the system.
4. Isotope production, transmutation, and/or activation for both radiation shielding and waste buildup.

In the energy regime of fusion neutrons, neutron scattering cross sections dominate the available nuclear reaction channels. Fusion neutrons, therefore, will lose energy from successive scattering collisions with different materials before being absorbed or leaking from the system. Accurately predicting the results from these elastic and inelastic scattering reactions is thus required to correctly predict the neutron flux in a fusion system. Experimental nuclear data for scattering reactions in the fusion energy range typically have large uncertainties due to the difficulty of experimentally separating elastic and inelastic scattering and determining the scattered neutron angular distributions.^[2]

Additionally, it is challenging to quantify experimental uncertainties for such experiments unless there are benchmarks for individual materials, for example, the Fusion Neutron Source (FNS) collection,^[3] and the OKTAVIAN experiments.^[4] These experiments use a DT neutron source emitting about 14-MeV neutrons to irradiate an assembly of interest and measure the subsequent neutron leakage. In some cases, activation foils were used to measure the internal neutron flux. These experiments, in particular, have provided foil dosimeter information in a certain fusion-related neutron flux. The DT neutron source used was pulsed to perform neutron leakage spectra measurements in time of flight, similar to the Lawrence Livermore National Laboratory pulsed sphere experiments,^[5] which have been used for nuclear data validation.

The quasi-differential (QD) neutron scattering method was developed at Rensselaer Polytechnic Institute (RPI) to provide data on neutron scattering cross sections, angular distributions, and outgoing neutron energy spectra. In contrast to the FNS-like experiments, the pulsed neutron source is a white energy source yielding a much larger and finer

experimental energy range. At an adequate flight path length, discrepancies between evaluated nuclear data and experiment can be observed in greater detail than can be achieved with a DT neutron source. Such experiments can be performed with materials that are important for fusion reactors and will provide insight into the most accurate evaluated nuclear data available, and where improvements in evaluated nuclear data sets are needed.

In this paper we review the QD neutron scattering method and provide examples of instances where evaluated nuclear data deficiencies have been identified and reevaluated to provide better agreement with the experimental data. The performance of the evaluated nuclear data for materials relevant to nuclear fusion systems were also investigated to determine where new experiments are needed.

II. MOTIVATION

Nuclear fusion reactors are complex structures that employ a wide variety of different materials, many of which are subjected to high-flux radiation environments. Figure 1 illustrates this complexity by including a simplified tokamak fusion reactor model.^[6] The evaluated nuclear data used to model neutron transport throughout the materials within a fusion system must all be accurate in order to obtain meaningful results. However, curating accurate evaluated nuclear data in the megaelectron-volt, or fast neutron region is challenging due to competition between several available decay channels and interaction mechanisms in the neutron-nucleus system, and the general lack of experimental nuclear data. Most evaluated nuclear data utilized during the design of nuclear fusion systems, therefore, are highly theoretical and in need of additional experimental constraints to ensure physical accuracy and plausible uncertainties.

An example of inconsistent evaluated incident neutron data in the megaelectron-volt energy region within major data libraries is provided in Fig. 2. In the figure, the leakage neutron flux from a DT source centralized within a homogeneous sphere of ^{182}W , a major isotope of an important material in nuclear fusion systems, was calculated using the spherical leakage model,^[6] an extension of previously reported results.^[7] Differences in excess of over 200% were observed between the JEFF-3.3^[8], JENDL-5.0^[9], and ENDF/B-VIII.0^[10] data sets above 0.1 MeV, far exceeding the typical evaluated uncertainties of about 5% for elastic and inelastic neutron scattering, respectively. Moreover, few nuclear data libraries considered in this analysis provide uncertainty on the angular distributions of secondary neutrons emitted from these reactions. Thus, for the purpose of this paper, we did not propagate covariance information to the simulated

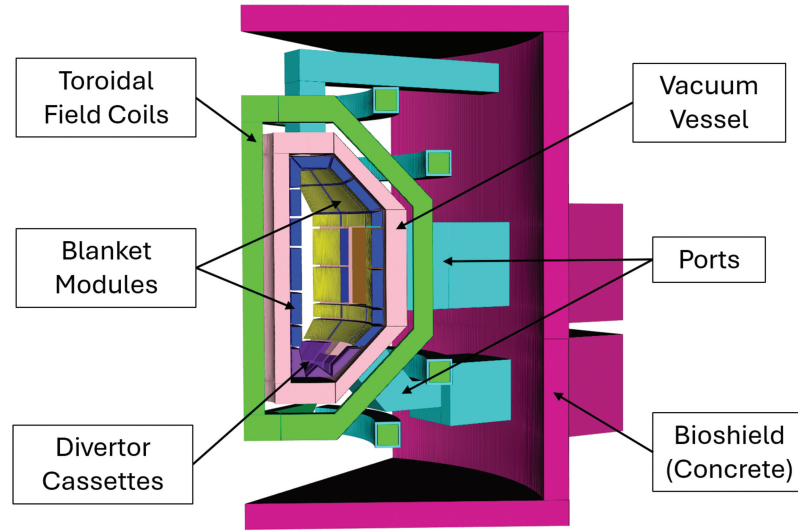


Fig. 1. Slice of a simplified tokamak MCNP model.

data, but only investigated central values. Implementation of nuclear data uncertainty propagation for fixed-source calculations into mainstream neutron transport codes is its own active area of research.^[11,12]

Evaluated nuclear data sets have been continuously improved since their inception in the 1950s/1960s due to advancements in both theoretical modeling of nuclear reactions and experimental capabilities. However, data within different evaluated nuclear data libraries may not always be physically accurate, or consistent, due to the lack of

experimental nuclear reaction data, deficient modeling, and/or data formatting techniques (Fig. 2). Furthermore, several data sets lack or provide minimal uncertainty and covariance data. Since little to no experimental nuclear data from nuclear fusion systems exist, computational benchmarks and tangential experiments are used to validate the accuracy of the evaluated nuclear data utilized for designing nuclear fusion systems. For the most recent release of the FENDL nuclear data library (FENDL3.2c), comparisons between the most recent evaluated nuclear data were

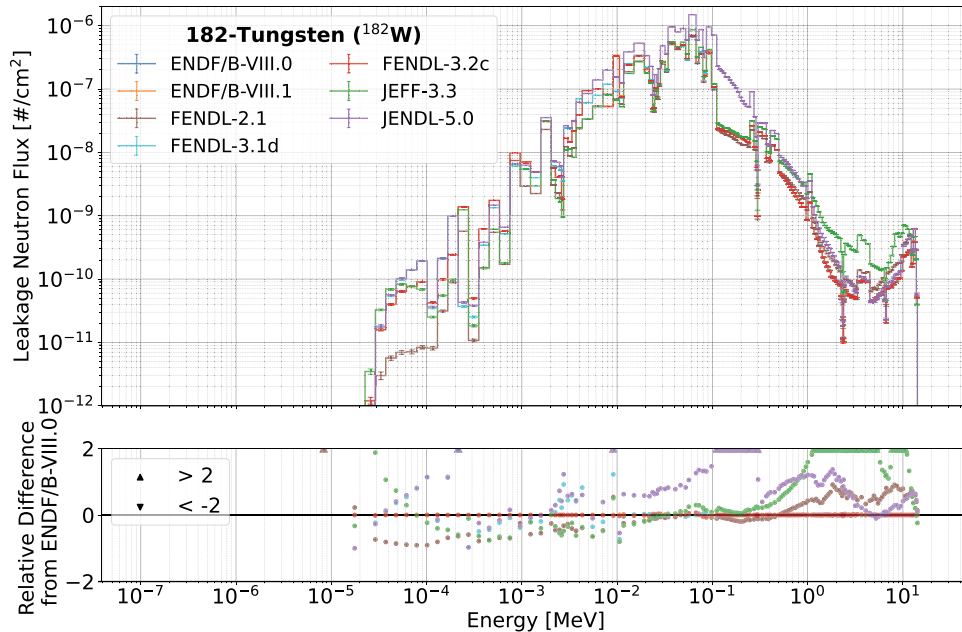


Fig. 2. Neutron leakage from ^{182}W modeled using the spherical leakage computational benchmark model and several evaluated nuclear data libraries.

made to several experiments for validation, with the majority of the experiments well reproduced by the FENDL-3.2c data, among other libraries.^[13]

Despite this, quantities such as the radial neutron flux and tritium production in accepted computational benchmarks remain highly inconsistent when computed using different evaluated nuclear data libraries. To demonstrate this, a one-dimensional (1-D) computational model from the International Thermonuclear Experimental Reactor (ITER) was considered.^[6,14] The radial neutron flux magnitude in this model was calculated using the ENDF/B-VIII.0, ENDF/B-VIII.1^[15], JEFF-3.3, JENDL-5.0, FENDL-2.1^[16], FENDL-3.1d^[17], FENDL-3.2c evaluated nuclear data libraries. Figure 3 provides the results of these calculations as a ratio to the legacy FENDL-2.1 library. Discrepancies on the order of $\pm 10\%$ are observed from perturbing the underlying nuclear reaction data library used to perform the neutron flux calculation.

The continuous production of nuclear fuel, which is commonly deuterium and tritium in nuclear fusion systems, is required to sustain nuclear fusion reactions. Therefore, the production of these isotopes within the breeding, or blanket, regions of a fusion reactor are crucial to the system design. Most proposed nuclear fusion reactor designs employ lithium (Li) or Li-based blanket materials due to the relatively high ${}^6\text{Li}(n,t)$ and ${}^7\text{Li}(n,Xt)$ reaction cross sections.^[18] The overall production of tritium and the tritium breeding ratio (TBR) in fusion systems is of particular concern due its relatively short half-life, low natural abundance, and high procurement cost.^[19] The reaction (or production) rate of tritium is directly

proportional to the neutron flux within the blanket. Therefore, 10% differences in neutron flux modeling from inconsistent nuclear data can substantially influence the production rate of tritium, and likewise, the TBR.

The radial neutron flux and tritium production utilizing the aforementioned evaluated nuclear data libraries have been calculated using two accepted computational benchmarks, the Helium-Cooled Pebble Bed Test Blanket Module (HCPB-TBM) and the Water-Cooled Lithium Lead Test Blanket Module (WCLL-TBM) ITER 1-D models,^[6,13] the results of which are presented in Fig. 4. Although the rate of tritium production in the blanket is sensitive to the ${}^6\text{Li}(n,t)$ cross section in these cases, it is a standard below 1 MeV^[20] and varies little above this energy in the evaluated nuclear data libraries considered. Therefore, other nuclear reactions perturbing the neutron flux in the breeder region, such as neutron scattering and other neutron-induced emission reactions with neutron multiplier, first-wall, vacuum vessel, and/or coil materials, such as O, Be, and Pb contribute to the differences observed in these calculations.

The discrepancies observed between evaluated nuclear data libraries in computational benchmarks, despite each considering several experimental data sets for evaluation and validation, emphasize the need for high-fidelity, differential validation experiments for fusion-related evaluated nuclear data sets. Since the neutron flux in fusion systems is highly sensitive to neutron scattering reactions above 0.5 MeV, the aforementioned QD neutron scattering method can provide additional experimental nuclear reaction data for

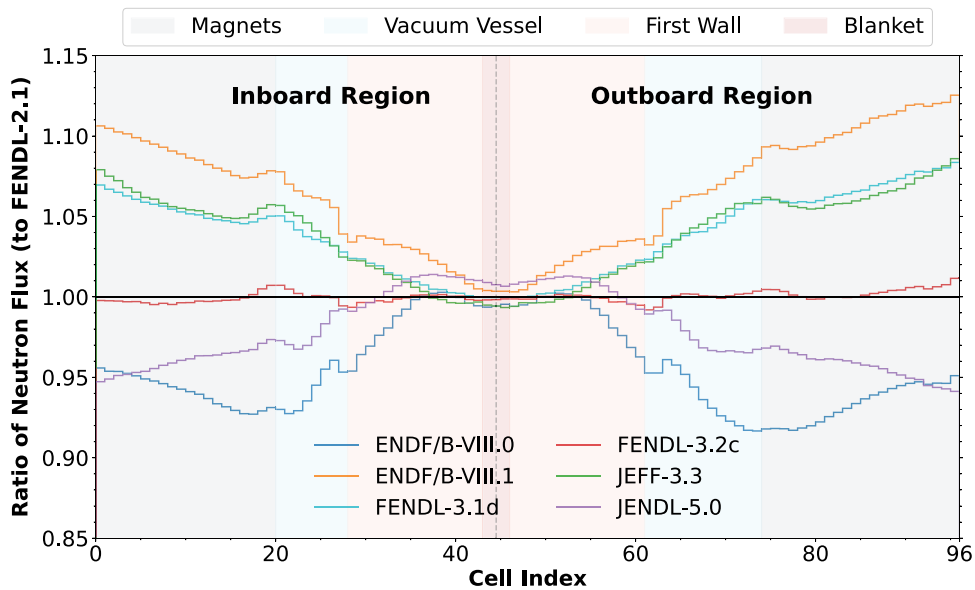


Fig. 3. Radial neutron flux modeled within the ITER 1-D computational benchmark model calculated using various evaluated nuclear data libraries.

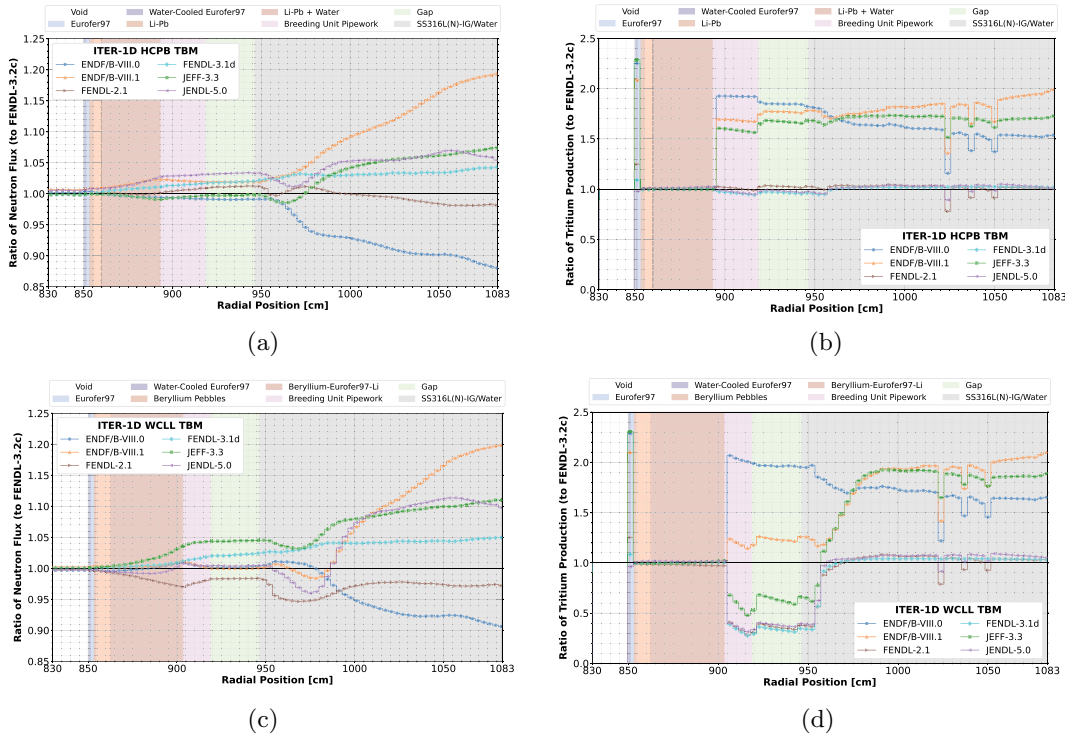


Fig. 4. Neutron flux and tritium production in the (a) and (b) ITER 1-D HCPB-TBM and (c) and (d) WCLL-TBM computational benchmark models utilizing several evaluated nuclear data libraries.

robust validation of future evaluated data sets. These experiments complement DT neutron source measurements well since previous and future DT source measurements can be compared to accelerator measurements to verify accuracy; while providing higher resolution experimental nuclear reaction data in additional energy regions prevalent in nuclear fusion systems.

III. THE QD SCATTERING METHOD

The QD scattering methodology was developed in tandem with the high-energy neutron scattering detector system at RPI to validate megaelectron-volt neutron scattering data for nuclear fission applications.^[21] Since the QD scattering methodology has been described in several previous measurements of both common structural materials, such as Mo,^[22] Zr,^[23] Fe,^[24] Cu,^[25] and actinides, such as ²³⁸U,^[26] ²³⁵U, and ²³⁹Pu,^[27] the methodology is discussed briefly here.

As previously mentioned, RPI QD neutron scattering measurements leverage the nearly isotropic pulsed white neutron source created with the RPI electron linear accelerator to perform neutron time-of-flight spectroscopy. Neutrons are produced in an unmoderated tantalum (Ta) target^[28] as the accelerated (~55 MeV) electrons slowdown in the Ta,

producing intense bremsstrahlung radiation, and subsequently, photoneutrons via the ¹⁸¹Ta(γ ,n) reaction. The resultant neutron spectrum from this target spans the high kiloelectron-volt to megaelectron-volt energy region, and can be described by a weighted sum of neutron evaporation spectra at varying energies.^[21] A typical geometry for a QD neutron scattering experiment is shown in Fig. 5.

In this setup, a sample of interest is located at distance L_1 from the neutron source and the neutron detectors are present at distance L_2 ; at RPI, these parameters are typically $L_1 = 30$ m and $L_2 = 0.5$ m. Therefore, the measured time of flight of a scattered neutron of resultant energy E_1 at any neutron detector is $t = t_1 + t_2$. The neutron-nucleus interaction time is assumed to be negligible. The kinetic energy of a measured neutron is determined using Eq. (1) by relating the measured time t the neutron took to travel the total distance L , where $L = L_1 + L_2$,

$$E = m_0 c^2 \left[\left(\sqrt{1 - \frac{\left(\frac{L}{t-t_0}\right)^2}{c^2}} \right)^{-1} - 1 \right], \quad (1)$$

and where

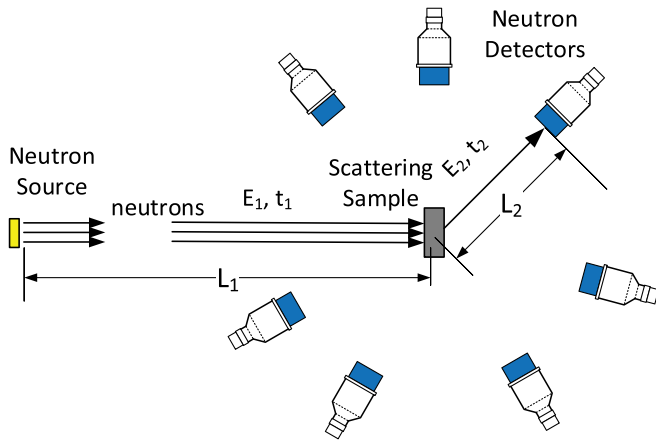


Fig. 5. QD neutron scattering experimental setup. (This figure is not to scale).

E = kinetic energy corresponding to a measured neutron time of flight t

m_0c^2 = rest mass energy of a neutron

L = total flight path length ($L_1 + L_2$)

t = measured neutron time of flight

t_0 = gamma flash arrival time (corrected for gamma-ray time of flight of distance L)

c = speed of light in vacuum.

Note that Eq. (1) yields only the approximate neutron energy since lethargy gained from a single or multiple scattering interactions with the sample is not included. In this case, the approximation is reasonable since $L_1 \gg L_2$.

Thick samples typically are measured at RPI to induce multiple scattering reactions, which both forces interactions with cross sections at lower energies and generally is more consistent with application. The measured quantity is the total neutron emissions from the sample as a function of both incident neutron energy and outgoing neutron angle. For nonfissile samples, the vast majority of the measured signal is scattered neutrons. However, above the neutron separation energy of a target nucleus, many neutron-emitting decay modes, such as $(n,2n)$ or (n,np) , become available and contribute to the measured signal. Thus, QD neutron-induced neutron emissions most accurately describe the measured quantity.

Additional methods are needed to differentiate neutron scattering events from these other neutron-emitting reactions, which increase the measurement uncertainty. For certain nuclei, it is possible to separate elastic and inelastic neutron scattering events.^[29] QD neutron scattering experiments are best suited for the validation of total neutron emissions (cross sections and angular distributions) in fast incident neutron

evaluations. Methods are also in development to provide similar validation for total gamma-ray emissions, which are important for gamma heating calculations.^[30]

The neutron detectors typically used in QD neutron scattering measurements are liquid scintillators. These detectors possess both a relatively high efficiency to detect mega-electron-volt neutrons and a fast response time (a few nanoseconds), leading to accurate time-of-flight measurements.^[31] A limitation of these detectors for neutron investigations is a large sensitivity to gamma rays. However, many pulse shape discrimination techniques have been developed to accurately separate the neutron and gamma-ray signals.^[29,32] The measured detector responses can subsequently be processed to histograms of neutron or gamma-ray counts as a function of time of flight for each detector (or each angle). These time-of-flight histograms are then compared with radiation transport simulations.

Additional information is required to accurately reproduce the experiment in simulation, such as the neutron flux shape as a function of energy and the relative neutron detector efficiency as a function of energy, for each detector. At RPI, the neutron flux shape has been measured experimentally using a fission chamber,^[26] and thus is relative to the standard ^{235}U fission cross section. The relative neutron detection efficiency of the liquid scintillators can be determined computationally using software, such as SCINFUL,^[33] or by experiment. It has been demonstrated at RPI that measuring the relative neutron detection efficiency profiles of each neutron detector allows for small differences between neutron detectors to be resolved.^[26] This is accomplished by placing each neutron detector directly in the neutron beam and comparing the measured detector response to the previously measured neutron flux. Due to these findings, an experimental approach is preferred when feasible.

At RPI, a sample of reactor-grade graphite (elemental carbon) is measured as part of any QD neutron scattering experiment. Since the double-differential scattering cross sections of carbon are well known, agreement between an experiment and simulation validate the neutron flux shape, neutron detector efficiencies, and simulated experimental geometry. Radiation transport simulations typically are performed using MCNP®, in this work version 6.3 was used,^{[34]a} with point

^aMCNP® and Monte Carlo N-Particle® are registered trademarks owned by Triad National Security, LLC, manager and operator of Los Alamos National Laboratory (LANL). Any third party use of such registered marks should be properly attributed to Triad National Security, LLC, including the use of the designation as appropriate. For the purposes of visual clarity, the registered trademark symbol is assumed for all references to MCNP within the remainder of this paper.

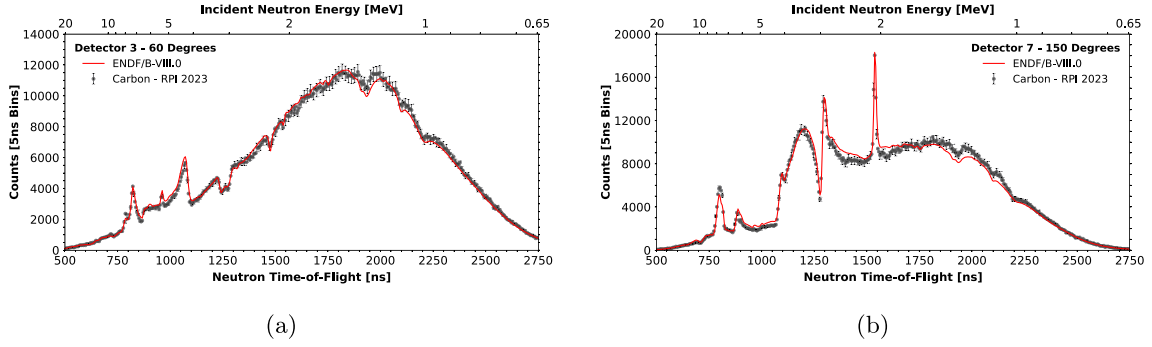


Fig. 6. Elemental carbon QD neutron scattering experiment versus the ENDF/B-VIII.0 evaluation from a recent RPI tantalum QD neutron scattering measurement.

detector (F5) tallies as a function of time. The agreement between recently measured carbon QD neutron scattering^[35] at forward and backward scattering angles are shown in Fig. 6. Note that the scattering angles are relative to the incident neutron beam. Generally, good agreement is observed for all time bins (or outgoing energies), which validates an experiment. The average difference observed between the carbon measurement and reference evaluation (ENDF/B-VIII.0 in this case) was adopted as the systematic uncertainty of the experiment and methodology. However, some minor differences can be attributed to the carbon cross sections, such as those between 6 to 8 MeV at backward angles.^[36,37]

Since only the shape of the neutron flux is measured at RPI, simulations must be normalized to the experimental quantities. Normalization factors for each neutron detector (angle) are determined by comparing the integrals of the time-of-flight histograms between the carbon experiment and simulation. A visualization of these normalization factors, relative to their average, is present in Fig. 7. This deviation has been observed to range from 3% to 8%. These normalization factors are then used to normalize the simulation of the measured sample of interest and the contribution of the open beam (background).

III.A. Results from Previous Measurements

Quasi-differential neutron scattering measurements, such as those performed in the megaelectron-volt energy range at RPI, provide a robust platform to validate evaluated nuclear data for applications. To demonstrate the value of these experiments, progressions made in nuclear data evaluations utilizing these experiments are discussed in this section.

III.A.1. Tantalum

A QD neutron scattering measurement was recently performed on a sample of elemental tantalum at RPI.^[35]

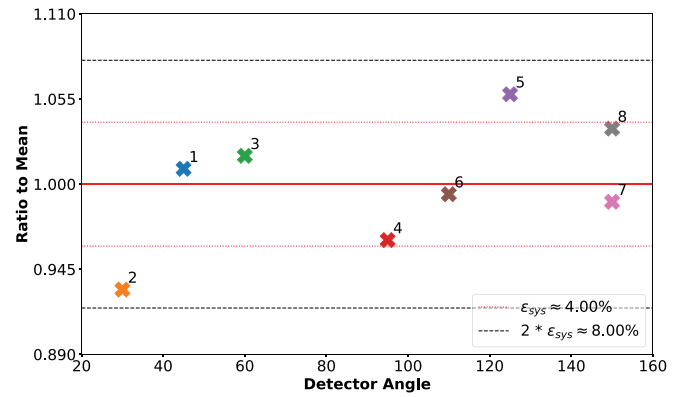


Fig. 7. Deviation of carbon area normalization factors from unity observed in a recent RPI tantalum QD neutron scattering measurement.

This measurement was performed to experimentally validate the new high-energy region incident neutron evaluation of ^{181}Ta in the recently released ENDF/B-VIII.1 evaluated nuclear data library. Neutron scattering was measured at seven unique scattering angles with an emphasis on backward scattering angles. Using the normalization factors and systematic error of this experiment, determined by measuring neutron scattering from a reference carbon sample (Figs. 6 and 7), the performance of several ^{181}Ta evaluated nuclear data sets was investigated.

The final measured neutron scattering spectra (corrected for deadtime and background) at select angles with corresponding radiation transport simulations are provided in Fig. 8. The results from both a forward (60-deg) and backward (150-deg) neutron scattering angle are provided. The ratios between the radiation transport simulation results and the experiment are also provided. The experimental findings demonstrate the utility of these experiments both as a validation platform and as a constraint for future ^{181}Ta evaluation efforts. Some significant takeaways from this experiment are the following:

1. Large discrepancies were present in neutron scattering channels of the modern ^{181}Ta evaluated nuclear data sets.

2. Using evaluated ^{181}Ta nuclear data from the ENDF/B-VIII.0 and/or JEFF-3.3 libraries in nuclear applications sensitive to neutron backscattering (or reflection) by ^{181}Ta between 0.75 MeV and 3 MeV will likely yield wrong answers.

3. The ENDF/B-VIII.1 and JENDL-5.0 ^{181}Ta evaluations agreed best with the experimental findings although smaller discrepancies remain. These data can be used to improve future ^{181}Ta incident neutron evaluations.

This experiment also highlighted that the FENDL-3.2c library may not always possess the most accurate evaluated nuclear data for neutron transport simulations in nuclear fusion systems. Despite good agreement at 60 deg between 1 MeV and 2 MeV, the FENDL-3.2c ^{181}Ta evaluation overpredicts the measured neutron scattering and emissions at backward angles at nearly all incident neutron energies.

Figure 9 is provided to further articulate these findings by comparing large energy regions of the simulated evaluated nuclear data to the experiment across all measured neutron scattering angles. Here, it is clear that the ENDF/B-VIII.1 and JENDL-5.0 evaluated ^{181}Ta nuclear data sets agree more so with the experiment compared to the FENDL-3.2c ^{181}Ta evaluation, particularly at backward angles, in both the nuclear fission (0.75 to 2.5 MeV) and fusion (5 to 15 MeV) energy regimes.

III.A.2. Lead

Lead is a key material used in blanket and neutron multiplier designs for nuclear fusion reactors.^[38] In support of next-generation fast neutron systems, a new incident neutron evaluation was performed on the major isotopes of Pb for the ENDF/B-VIII.1 nuclear data library.^[39] This new evaluation highlighted the utility of QD neutron scattering data to nuclear data evaluators during the evaluation

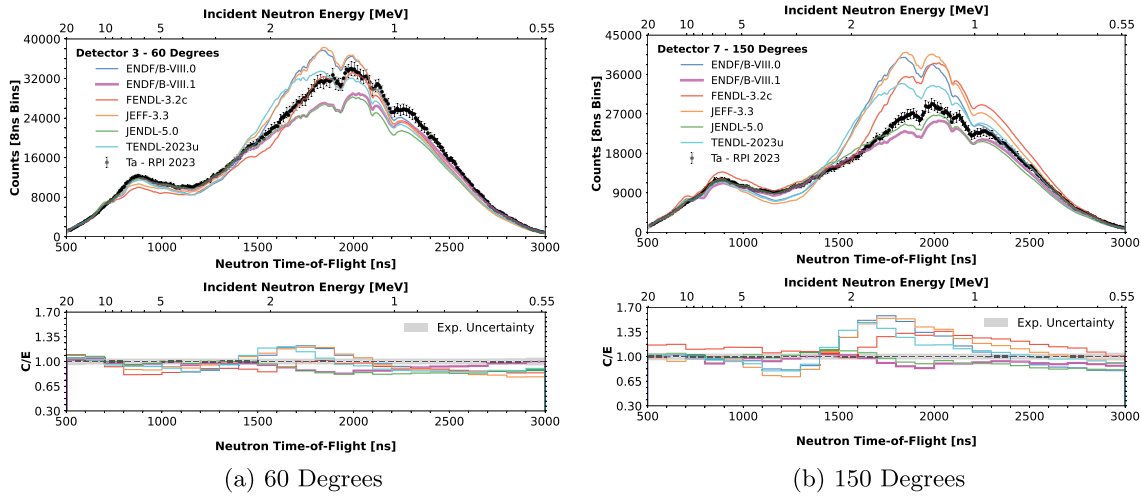


Fig. 8. Experimental elemental tantalum QD neutron scattering compared to simulation.

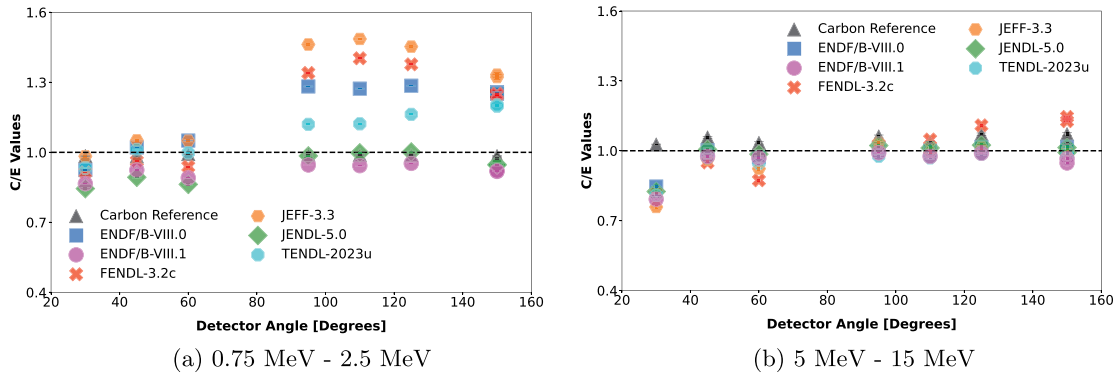


Fig. 9. Ratios between radiation transport simulations of several evaluated ^{181}Ta nuclear data sets and the RPI QD Ta neutron scattering measurement in both nuclear fission and fusion applicable energy regions.

process^[40] since QD neutron scattering data collected on elemental Pb at RPI^[41] were considered.

In this case, the QD neutron scattering data were leveraged for resonance spin assignment verification, which subsequently allowed the fidelity of the ^{208}Pb elastic scattering angular distributions to be enhanced via the Blatt-Biedenharndt formalism.^[40] Figure 10 illustrates the improved agreement between the experiment and the new ENDF/B-VIII.1 Pb evaluation compared to both the previous ENDF/B-VIII.0 evaluation and other Pb evaluated nuclear data sets at a neutron scattering angle of 150 deg relative to the incident neutron beam.

IV. PROSPECTIVE RPI QD NEUTRON SCATTERING MEASUREMENTS

To demonstrate the applicability of RPI QD neutron scattering measurements to nuclear fusion system development, the evaluated nuclear data sets of materials lacking QD neutron scattering data were investigated. A summary of the materials considered along with their respective relation to and/or current use in nuclear fusion system designs is provided in Table I. The evaluated nuclear data (high kiloelectron to megaelectron-volt neutron scattering and neutron emissions) for a particular material were investigated by performing the radiation transport simulation portion of a QD neutron scattering experiment. These simulations used a 6-cm right cylindrical sample of natural abundance (unless stated otherwise), in a simplified geometry of the RPI QD neutron scattering experimental setup.

Evaluated nuclear data from the ENDF/B-VII.1,^[42] ENDF/B-VIII.0, ENDF/B-VIII.1 ($\beta 4$), FENDL-3.2c,

JENDL-4.0,^[43] JENDL-5.0, JEFF-3.3, and TENDL-2023^[44] libraries were considered in this analysis. Generally, differences of approximately 20% were observed within the experimental energy region (~ 0.5 to 20 MeV) for all the materials investigated, although multiple discrepancies in excess of 50% were also found. To first order, these discrepancies far exceeded typical evaluated uncertainties (ranging from about 2.5% to 10%, when available) for elastic and inelastic neutron scattering reactions in this energy region.

The results from some high-importance materials to fusion system design are discussed in this section. The results from the remaining materials investigated are provided in the Appendix. Evaluated nuclear data uncertainties and covariance data were not thoroughly investigated in this analysis. The primary objective of these experiments was to constrain and/or validate the accuracy of cross sections and angular distributions of neutron scattering and emission reactions. Once QD experimental data are available, evaluations can be validated within the reported experimental uncertainties.

IV.A. Silicon

Silicon (Si) is a leading candidate material, in the form of silicon carbide (SiC),^[45] for use as a first-wall barrier material in fusion reactors and as a blanket material in the form of Li_4SiO_4 .^[18] Si is also a primary constituent of concrete. Thus, Si will be subject to a high flux of 14-MeV neutrons, but also neutrons of lower energy returning from reflection or emission in other materials, such as the blanket and shielding. Therefore, to accurately model the neutron flux in the fusion system, neutron scattering and emission reactions with silicon must be well understood. However, it has been discovered that significant discrepancies exist between the evaluated Si

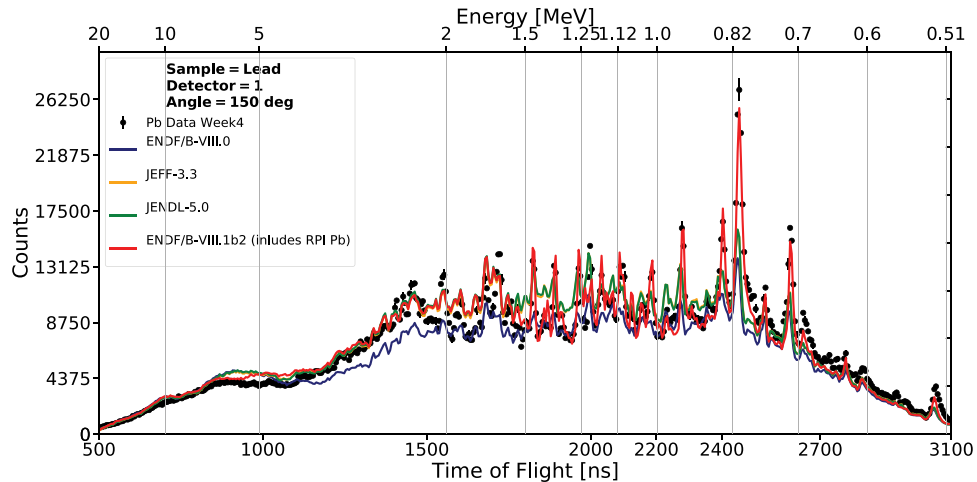


Fig. 10. Experimental lead QD neutron scattering compared to simulation. (Reproduced from Ref. [37] with permission).

TABLE I

Materials Present in Nuclear Fusion System Designs Which Lack RPI QD Neutron Scattering Data

Fusion Reactor Component	Element/Isotope	Proposed Concepts
Tritium breeding (blanket)	${}^6,{}^7\text{Li}$, O, Ti, Mg, Cl, Na, Si, K, Al	Li_2O – Steady-state tokamak reactor (SSTR, ^[18,53,97,98] compact tokamak reactor ^[95] , Li_2TiO_3 – HCPB/ Demonstration Power Plant (DEMO)/ITER-TBMs ^[18,96,54–56] , Japan Atomic Energy Research Institute (JAERI) advanced steady-state tokamak reactor (A-SSTR2) ^[18,53] , Li_4SiO_4 – HCPB ^[18,96] Pb-17Li – WCLL, ITER-WCLL-TBM ^[18,55,57,58] , DEMO ^[57,59,60] , FZK dual coolant blanket concepts (DC) ^[61] , ARIES* Advanced Tokamak (AT) ^[62,63] , Other Li-based concepts – ARIES-I ^[64] ARIES Reverse Shear (RS) ^[65] , Evaporation of Lithium and Vapor Extraction (EVOLVE) ^[66,67] F-based salts such as FLiBe in the Force Free Helical Reactor (FFHR-2) ^[18,68] , FLiNaBe ^[69,70] , and FLiNaK ^[71] , Cl-based salts ^[72]
Magnets and/or coils	Sn, Nb, Ti, Y, Ba, Ti	Nb_3Sn ^[50,73,74] , NbTi ^[75] – ITER/DEMO ^[76] Yttrium barium copper oxide (YBCO) ^[51,74] Rare-earth barium copper oxide (RBCO) – Commonwealth Fusion Systems SPARC tokamak reactor ^[77,78]
Shielding	W, B, Si, Hf, H_2O	W ^[47,73,79–81] , WC alloys ^[47,82] , WB-alloys ^[47,83] , Hf ^[84] , SiC (first wall) ^[18,73,80] , B_4C ^[18,47,73,80]
Structural materials	Si, Al, V, Ni, Cr, O, Co, Mn, N, Ca, S, K, Mg	SiC ^[18,45,73,79,86] , ferritic/martensitic steels ^[18,79,86] , Reduced activation ferritic steels (RAFS) ^[18,85,86] such as Eurofer97 ^[73,85,88] , V-alloys ^[79] such as: V-4Cr-4Ti-CaO ^[52] , V15-Cr-5Ti ^[52] , V-Cr-Mn ^[89] , and V-Cr-Mn-Ti ^[89] , Stainless steels (austenitic, SS 316 L, etc.) ^[73,85] , Al alloys ^[85,90] , Concrete ^[91,92] , Insulators such as MgO , Al_2O_3 , MgAl_2O_4 ^[73,85,94]
Coolant**	H_2O , He, Li, FLiBe, Bi	Pb-Bi eutectic ^[93] , Pb-Li eutectic (Pb-17Li) ^[18,55,57,58] , H_2O (ITER WCLL-TBM & DEMO) ^[18,55,57,58] , He (ITER HCPB-TBM & DEMO) ^[18,55,58,96]

*The advanced reactor innovation and evaluation study (ARIES) was a collaborative US research and development effort centered around the advancement of fusion reactor technologies.

**Note that certain fusion reactor concepts are self-cooled by a liquid breeder such as Pb-17Li.

nuclear data sets. Radiation transport simulations corresponding to a hypothetical QD neutron scattering measurement at RPI of a pure Si metal sample are presented in Fig. 11.

The results from these calculations demonstrated that large differences exist among the evaluated Si double-differential neutron scattering cross section data. These differences can propagate to vastly different tally scores in a system sensitive to Si megaelectron-volt neutron scattering simply by changing the evaluated Si nuclear data used. Ultimately, these discrepancies introduce additional uncertainty to the calculated parameter(s) of interest. Since there is a large amount of Si in nuclear fusion systems (first wall, concrete, structural materials), Si nuclear data are important for accurate neutronics modeling of the system.

IV.B. Lithium, Titanium, and Oxygen

Sustaining a nuclear fusion reaction requires that adequate fuel be available in the system. A DT fusion system, for example, requires significant quantities of both deuterium and tritium in the system continuously. Since replenishing tritium used in nuclear fusion is prohibitively expensive via procurement, it is necessary that fusion reactors breed enough tritium to sustain the nuclear fusion reaction. Tritium breeding occurs in the blanket, which typically contains large amounts of Li due to the large ${}^6\text{Li}$ (n,t) cross section. A material being developed for blankets is Li_2TiO_3 .^[46]

Calculations of the neutron flux in the breeder/blanket region must be accurate to ensure proper calculations of both

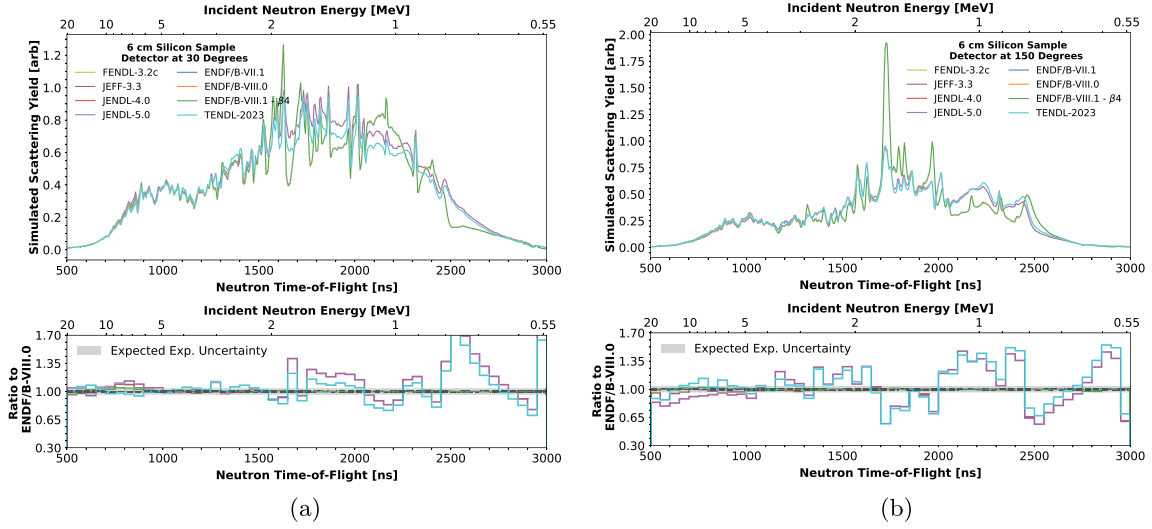


Fig. 11. Radiation transport simulations corresponding to hypothetical QD neutron scattering measurement of silicon at RPI.

the amount of tritium needed to sustain the fusion reaction, and the amount of tritium being produced. However, this cannot be achieved unless adequate nuclear data for these materials are used in radiation transport simulations. An investigation of current the ${}^6\text{Li}$, Ti, and O evaluated nuclear data sets was performed to determine if QD neutron scattering data are needed to further constrain the evaluated quantities. The results from the ${}^6\text{Li}$ simulations are presented in Fig. 12.

Discrepancies in the evaluated neutron scattering and emission data for ${}^6\text{Li}$, particularly above 5 MeV, were observed. Without additional ${}^6\text{Li}$ experimental data, such as QD neutron scattering data, it is unclear to users which evaluated nuclear data library will model the neutron interactions with ${}^6\text{Li}$, and thus, the neutron flux and tritium production in the blanket, most accurately. Additional uncertainty in the neutron flux and reaction rate calculations is introduced as additional materials, possessing similarly inconsistent evaluated nuclear data, are included. This is the case with Li_2TiO_3 fusion blankets since differences in excess of 40% were observed between the evaluated neutron scattering and emission data of titanium (Fig. 13) and oxygen (Fig. 14) in multiple energy regions. Oxygen is also present in significant quantities in concrete where differences in neutron scattering reaction rates can manifest into improper activation and shielding calculations.

IV.C. Tungsten

Several types of ionizing radiation are present in large quantities within a nuclear fusion system. Properly shielding and containing this radiation is needed to reduce the dose to both personnel and the radiation-sensitive components. Accurate modeling of neutron scattering interactions within

shielding materials is needed to first predict the magnitude and energy distribution of both the neutrons and gamma rays (from inelastic scattering or other neutron emitting reactions) to be attenuated, and then to determine the necessary amount of shielding required to obtain the required dose rates beyond these shielding materials at different times.

A primary material candidate for radiation shielding in fusion systems is tungsten due to its desirable mechanical and chemical properties^[47] and high gamma-ray attenuation coefficient. Tungsten is also considered to be a candidate material for first-wall containment.^[48] Radiation transport simulations were performed on a sample of tungsten in the RPI high-energy neutron scattering system to assess the consistency of available evaluated neutron scattering and emission data (Fig. 15). Discrepancies between the evaluated nuclear data were observed, particularly at backward scattering angles, and ranged between 5% to 40% above 1.5 MeV.

Performing a QD neutron scattering experiment on tungsten will complement existing shielding and leakage experiments^[4,49] by providing higher-resolution nuclear reaction data over a large energy range. This will enhance the validation of evaluated tungsten nuclear data sets and improve the accuracy of the shielding and dosimetry calculations of fusion systems.

IV.D. Niobium

To confine and manipulate the highly dynamic plasma in a nuclear fusion reactor, large superconducting magnets and coils are used to create strong magnetic fields (> 10 T). Most modern magnetic confinement fusion reactor designs

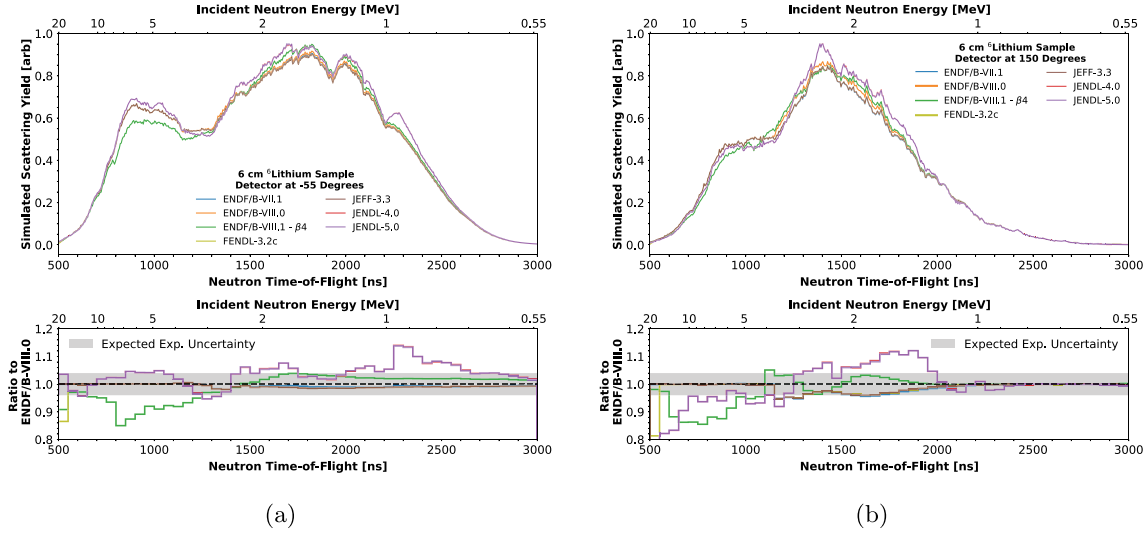
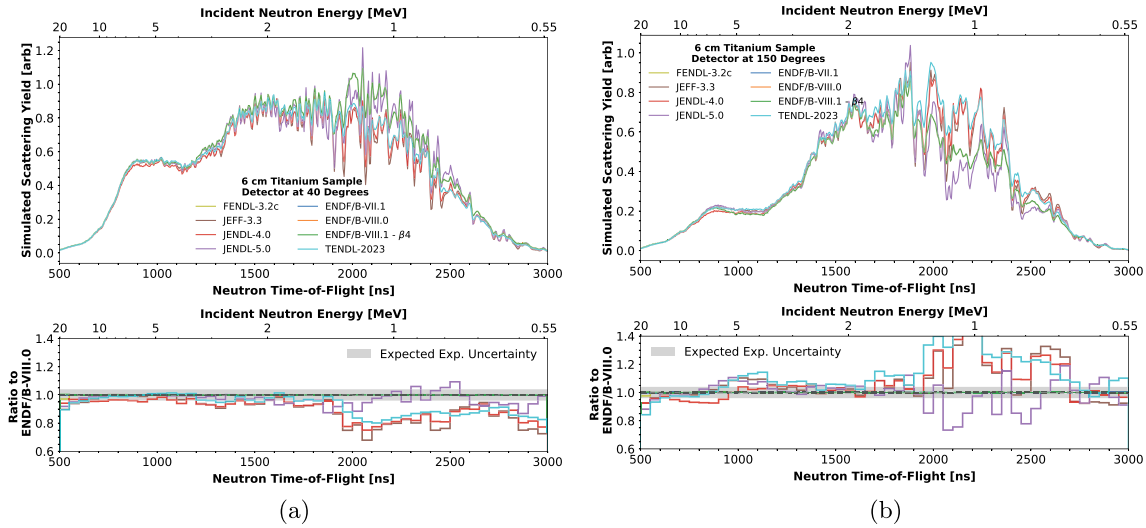
Fig. 12. Radiation transport simulations corresponding to hypothetical QD neutron scattering measurement of ${}^6\text{Li}$ at RPI.

Fig. 13. Radiation transport simulations corresponding to hypothetical QD neutron scattering measurement of titanium at RPI.

leverage powerful Nb_3Sn superconducting magnets and coils^[50] alongside other superconducting materials, such as $\text{YBa}_2\text{Cu}_3\text{O}_7$ (YBCO) for wires and coatings.^[51]

Neutron scattering and reflection from the superconducting magnets and coils will affect the neutron flux of a fusion device. Both Nb and Sn evaluated nuclear data were investigated by performing radiation transport simulations of a QD neutron scattering experiment at RPI; the Nb results are provided in Fig. 16. At energies above 2 MeV, discrepancies on the order of 30% were observed in the Nb evaluated neutron scattering and emission data at both forward and backward scattering angles. The results from the Sn evaluated nuclear data sets are provided in the Appendix.

IV.E. Vanadium

The extreme conditions within a nuclear fusion reactor require the development and testing of new materials to withstand these environments. The suitability of different ferritic and martensitic steels, as well as those alloyed with large amounts of vanadium (V), has been studied extensively for fusion systems.^[45,52] Implementation of V-alloyed steels into the structure of a fusion system introduces an additional dependence of the neutron flux on evaluated vanadium cross-section data.

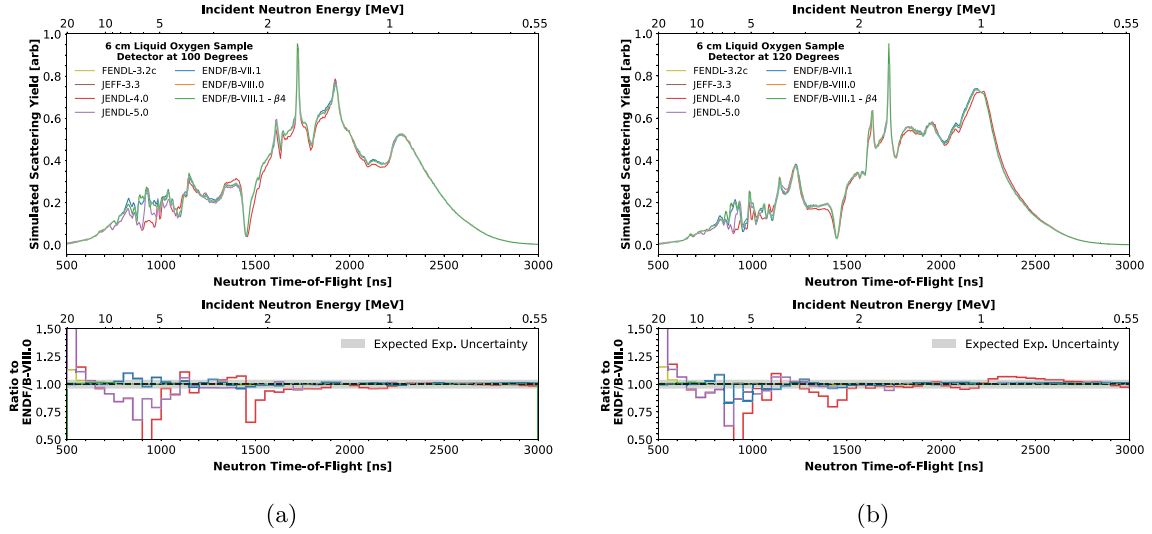


Fig. 14. Radiation transport simulations corresponding to hypothetical QD neutron scattering measurement of liquid oxygen at RPI.

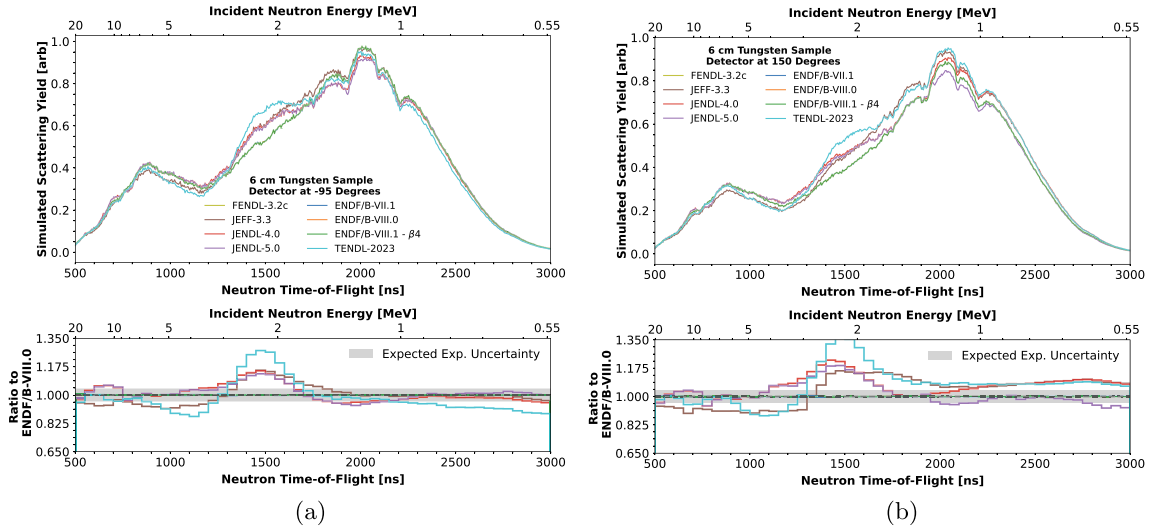


Fig. 15. Radiation transport simulations corresponding to hypothetical QD neutron scattering measurement of tungsten at RPI.

Figure 17 presents the results from radiation transport simulations using various vanadium evaluated nuclear data sets, revealing discrepancies of over 15% in total neutron scattering at forward and backward angles. The total neutron emissions from vanadium can be validated, and regions of disagreement resolved, with QD neutron scattering experimental data.

V. CONCLUDING REMARKS

Accurate modeling of radiation transport in nuclear systems requires accurate nuclear reaction data. To validate the evaluated nuclear data used in applications, experiments are performed to observe the agreement

between the theoretical models and experimental data. Despite the extensive evaluation and validation efforts put forth in both fusion-specific (FENDL) and general purpose (ENDF/B, JEFF, JENDL, TENDL) nuclear data libraries, significant differences in neutron cross sections and angular distributions remain between these evaluated nuclear data sets.

In several instances these differences impact nuclides which are important to nuclear fusion applications. Therefore, when different evaluated nuclear data are used to model quantities paramount to nuclear fusion reactor design, such as neutron flux and tritium production, inconsistent results are obtained that far exceed the evaluated uncertainties when they are available (Sec. II). These inconsistencies not only introduce

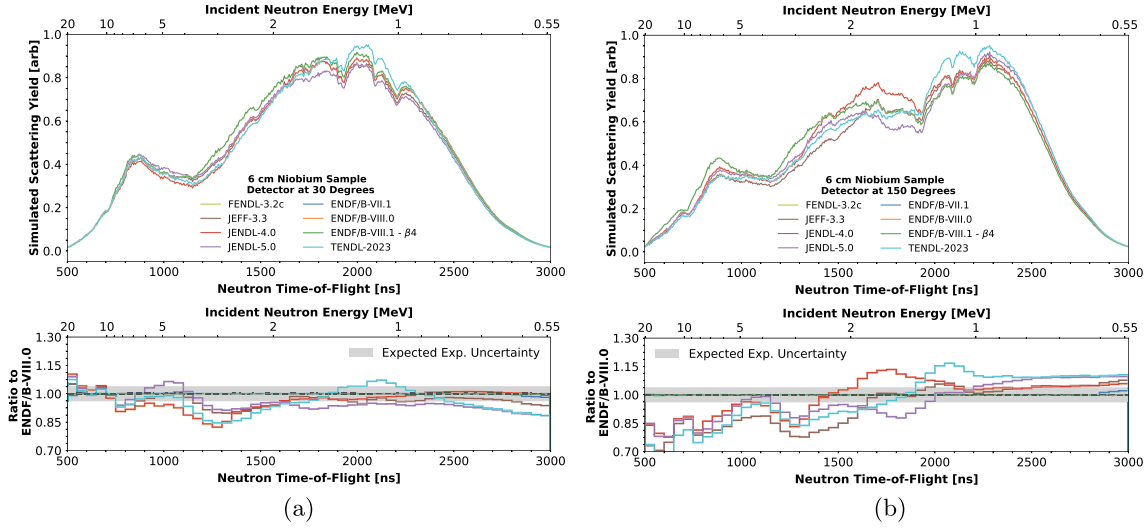


Fig. 16. Radiation transport simulations corresponding to hypothetical QD neutron scattering measurement of niobium at RPI.

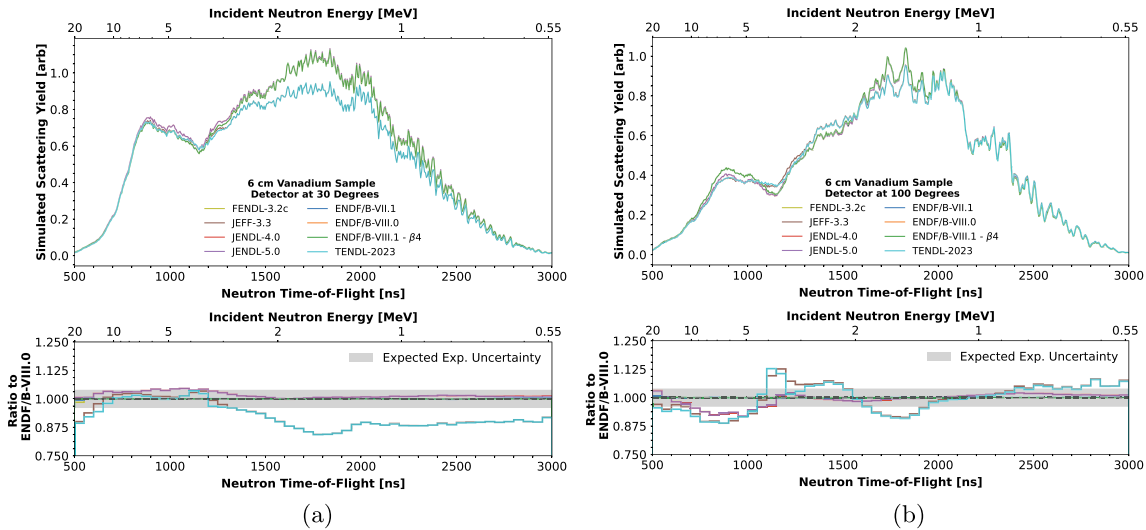


Fig. 17. Radiation transport simulations corresponding to hypothetical QD neutron scattering measurement of vanadium at RPI.

additional uncertainty to the parameter of interest, but also confusion as to which calculation is most physically accurate. Several of these inconsistencies between evaluated data arise from discrepancies in elastic and inelastic neutron scattering cross-section and angular distribution data, which are difficult to accurately model and evaluate without experimental data. The QD neutron scattering experimental methodology is as an efficient platform yielding high-fidelity, differential nuclear reaction data for the validation of nuclear data evaluations, such as those produced recently for tantalum (Sec. III.A.1).

The agreement of neutron scattering reaction data for nuclides of relevance to nuclear fusion applications between

the ENDF/B-VII.1, ENDF/B-VIII.0, ENDF/B-VIII.1 (β_4), JEFF-3.3, JENDL-5.0, TENDL-2023, and FENDL-3.2c evaluated nuclear data libraries was investigated and many inconsistencies were identified. This analysis was performed using MCNP6.3 radiation transport simulations of each material in the RPI experimental high-energy neutron scattering system.

The most noteworthy disagreement in the neutron scattering simulations was that of up to 75% between evaluated Si nuclear data sets at backward ($\theta > 90$ deg) neutron scattering angles between 0.5 MeV and 20 MeV. Additional discrepancies on the order of 20% to 50% were found in several key materials utilized in nuclear fusion applications, those being W, Nb, V, Li, Ti, O, Mg,

Ca, Al, Cr, Bi, K, etc. (see both [Sec. IV](#) and the [Appendix](#)). These discrepancies introduce significant additional sources of uncertainty in radiation transport simulations of fast nuclear systems sensitive to these materials, as the differences observed surpass the evaluated nuclear data uncertainties to first order when provided. Future investigations, including prorogation of available nuclear data uncertainties of these materials in QD scattering calculations, should be conducted once tools are made available to perform such analyses.

It is important to distinguish consistencies observed between evaluated nuclear data libraries and accuracy. Intuitively, consistency between the evaluated nuclear data sets, particularly within quoted uncertainties, suggests that the data are accurate. However, in the absence of appropriate experimental nuclear reaction data, the merit of evaluated quantities is ambiguous. Thus, new nuclear data measurements employing the QD scattering methodology are recommended to validate the accuracy of the evaluated nuclear data sets for materials pertinent to nuclear fusion system design and application ([Table I](#)). Such validation enables a reduction in the uncertainty of model calculations, such as the energy distribution and magnitude of the neutron flux, reaction rates, nuclear heating, isotope production and tritium breeding, neutron multiplication, activation, shielding requirements, and dose rates in nuclear fusion systems.

APPENDIX

RESULTS FROM ADDITIONAL PROSPECTIVE RPI QD NEUTRON SCATTERING MEASUREMENTS

This appendix includes brief results from the radiation transport simulations considering the materials specified in [Table I](#) that were not explicitly discussed in [Sec. IV](#). All the materials considered were composed of the natural composition of the element(s) unless otherwise specified. For most materials, both a forward and backward neutron scattering angle are provided.

A.I. ALUMINUM

Aluminum is used ubiquitously across the nuclear industry as a structural material for varying applications including nuclear fusion systems ([Table I](#)). Aluminum oxide (Al_2O_3) can also be used as an insulator. The simulated neutron scattering yields from different evaluated aluminum nuclear data at forward and backward neutron scattering angles are provided in [Fig A.1](#) where discrepancies of 10% to 20% are observed between 1 MeV and 5 MeV.

A.II. BARIUM

Barium is a constituent of yttrium barium copper oxide (YBCO) super conductors, which are under

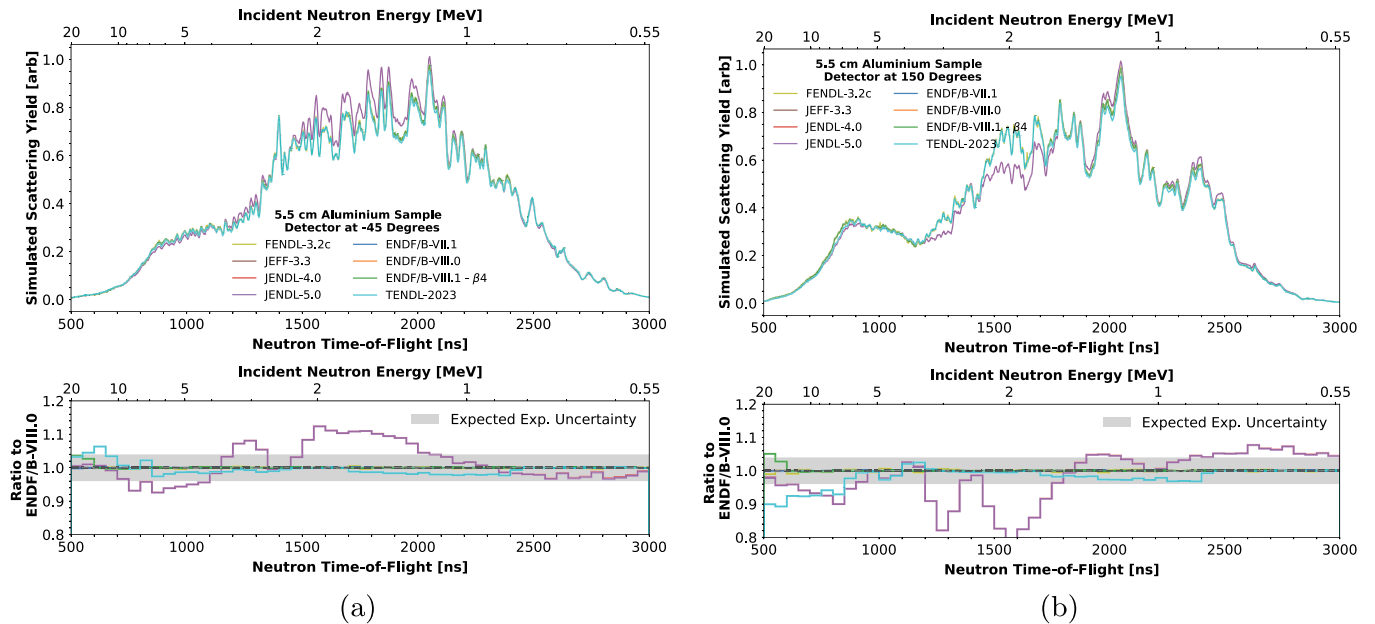


Fig. A.1. Expected computational results of several evaluated nuclear data libraries corresponding to a QD neutron scattering measurement of aluminum at RPI.

development for use in nuclear fusion reactors (Table I). Substantial differences between the simulated neutron scattering yields from different evaluated barium nuclear datasets below 3 MeV are shown in Fig A.2.

A.III. BORON

Boron is a strong absorber of thermal neutrons and is used in shielding applications in several nuclear applications including prospective nuclear fusion reactors (Table I) where it can be subject to appreciable fluences of fast neutrons. Large differences in the simulated neutron scattering yields predicted by differ-

ent boron evaluated nuclear datasets are present above 3 MeV for both forward and backward neutron scattering angles are visible in Fig. A.3. Additional differences of about 10% are observed at forward scattering angles below 1 MeV.

A.IV. BISMUTH

Bismuth is an integral component to the Pb-Bi eutectic coolant concept for use in nuclear fusion reactors (Table I). In Fig. A.4, differences on the order of 20% between the simulated neutron scattering yields using different bismuth evaluated nuclear datasets

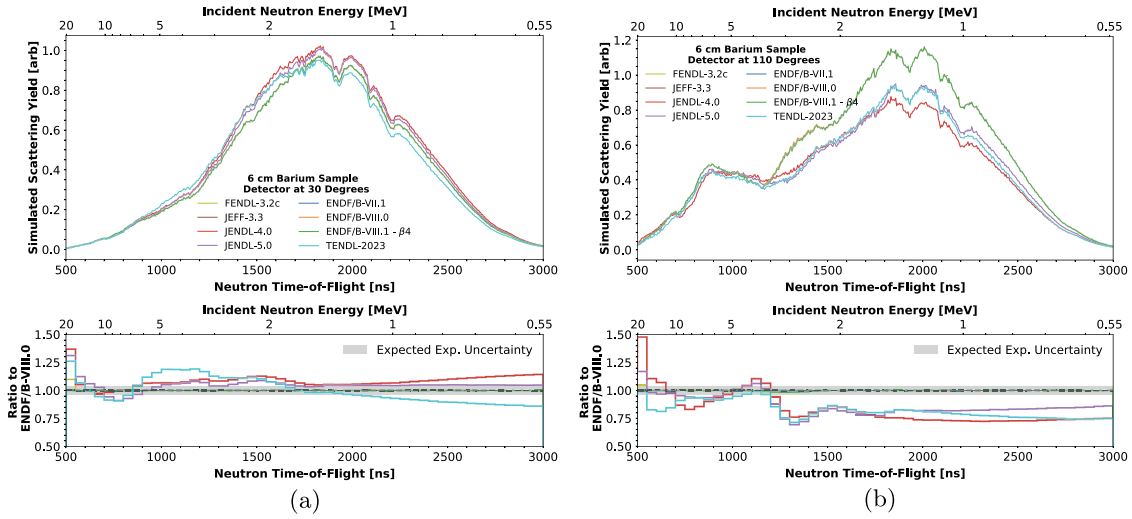


Fig. A.2. Expected computational results of several evaluated nuclear data libraries corresponding to a QD neutron scattering measurement of barium at RPI.

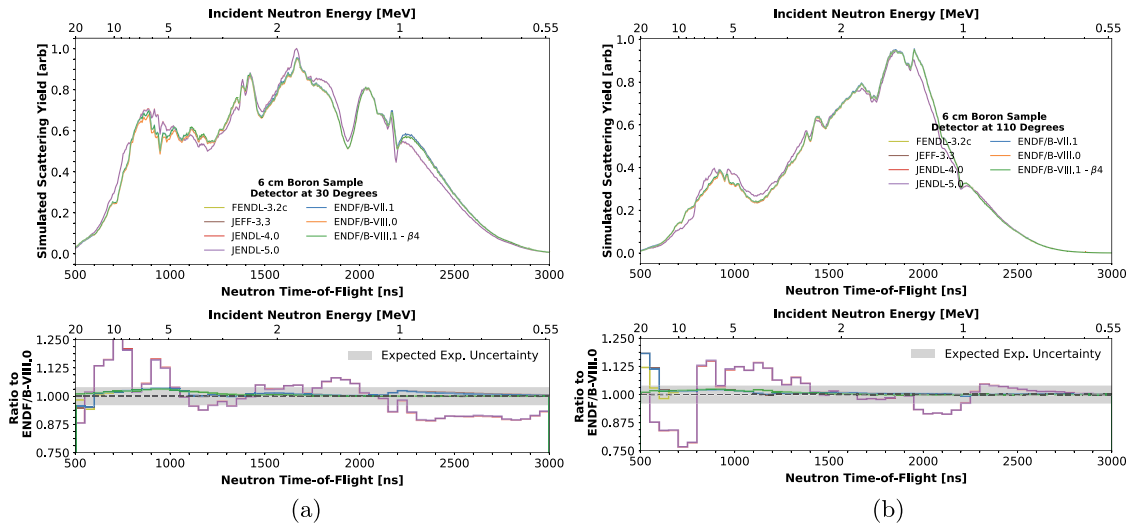


Fig. A.3. Expected computational results of several evaluated nuclear data libraries corresponding to a QD neutron scattering measurement of boron at RPI.

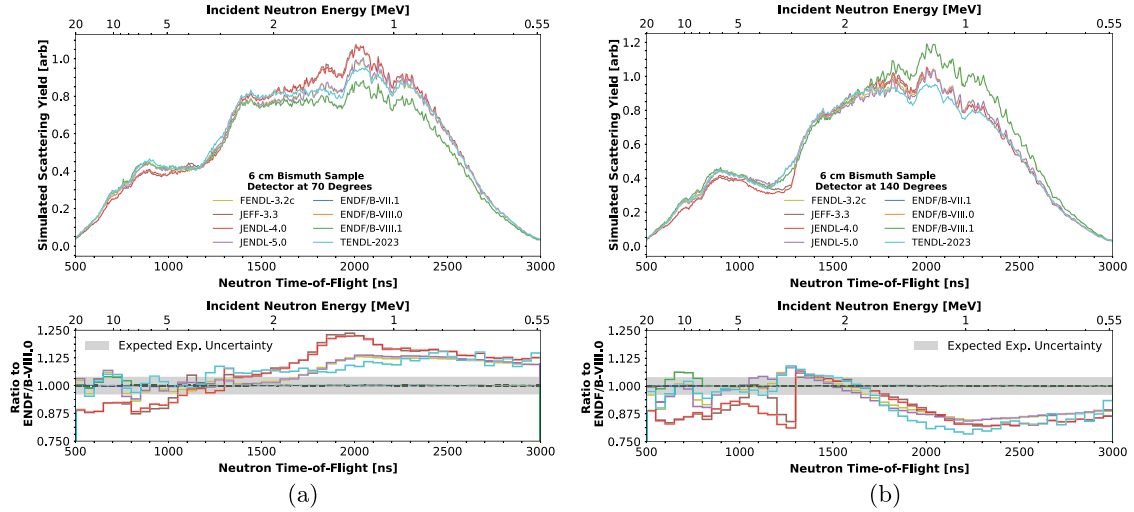


Fig. A.4. Expected computational results of several evaluated nuclear data libraries corresponding to a QD neutron scattering measurement of bismuth at RPI.

spanning most of experimental energy region (~ 0.5 MeV to 20 MeV) are observed. An unusually rapid drop in scattering yields calculated using the JEFF-3.3 and JENDL-4.0 libraries is also observed at 3 MeV at backward scattering angles.

A.V. CALCIUM

Calcium is present both in advanced steels under development for the construction of nuclear fusion reactors and in concrete (Table I). It is observed in Figure A.5 that significant discrepancies (exceeding 75% below 2 MeV) are present between the simulated neutron scattering yields from

different nuclear data libraries due to the conflicting representations of the large resonances of calcium at both forward and backward neutron scattering angles. Sample containment was not considered for this calculation.

A.VI. CHLORINE

Chlorine is present in many salt compounds proposed for use in both nuclear fusion (Table I) and generation-IV nuclear reactor concepts. To maximize chlorine atom density in a prospective measurement, a liquid sample of carbon tetrachloride (CCl_4) was considered. In Figure A.6, disagreement which exceeds

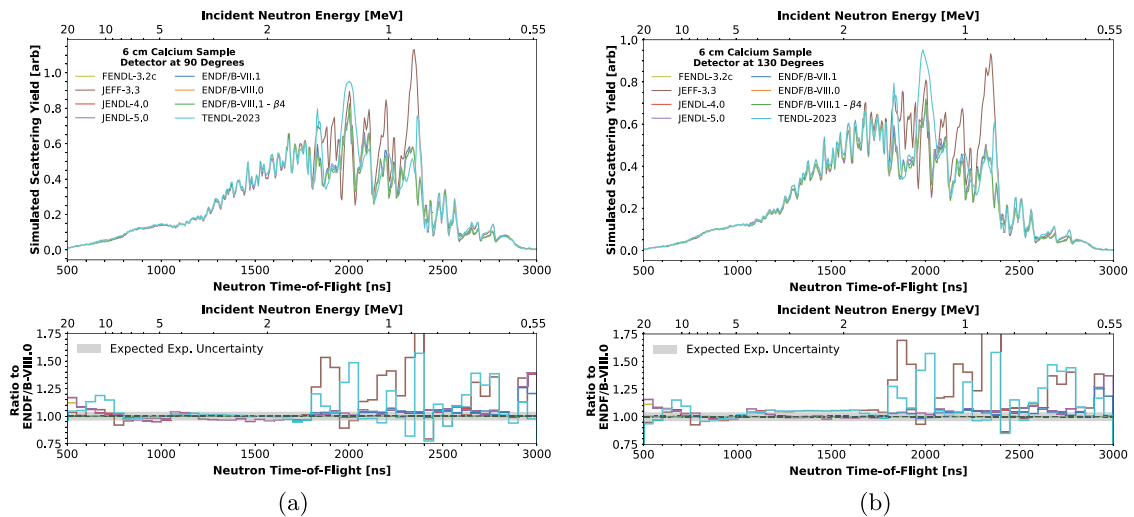


Fig. A.5. Expected computational results of several evaluated nuclear data libraries corresponding to a QD neutron scattering measurement of calcium at RPI.

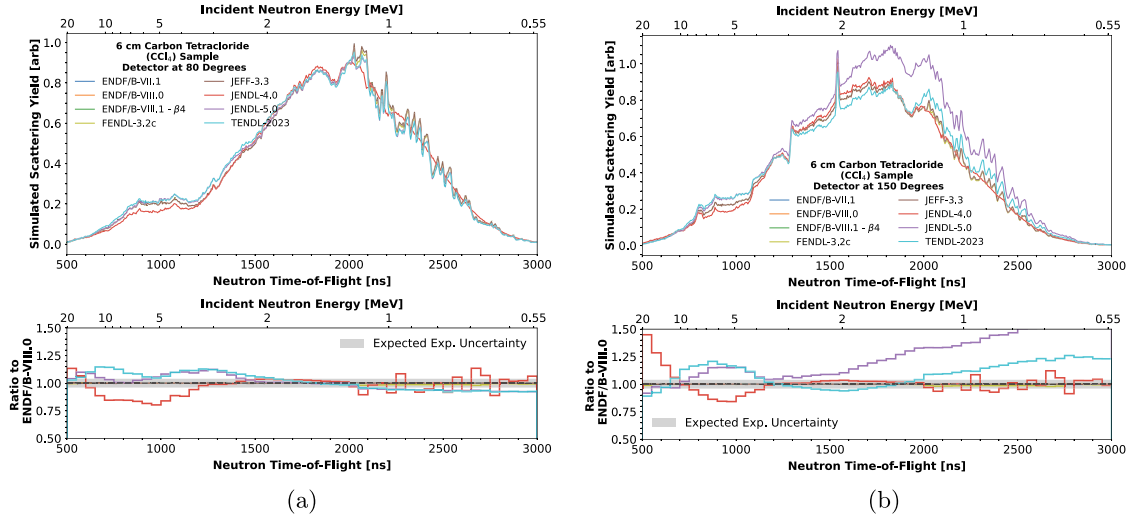


Fig. A.6. Expected computational results of several evaluated nuclear data libraries corresponding to a QD neutron scattering measurement of carbon tetrachloride at RPI, varying chlorine nuclear data only.

50% between the different chlorine evaluated nuclear datasets investigated is observed below 2 MeV at backward neutron scattering angles. Only chlorine nuclear data were varied in this calculation, and sample containment was not considered.

A.VII. CHROMIUM

Chromium is a primary constituent of several types of stainless steels (ferritic, martensitic, austenitic) due to its high strength and corrosion resistance. V-alloyed steels in development for fusion systems, likewise, contain large amounts of

chromium (Table I). In Fig. A.7 it is observed that the differences in representation of the strong resonance structure of chromium below 1.5 MeV by the evaluated nuclear datasets analyzed can propagate to differences in the neutron scattering yield of over 40%.

A.VIII. COBALT

Cobalt can be used as an alloying material for high strength steels which may be used in the construction of nuclear fusion systems (Table I). Differences of approximately 10% in the simulated

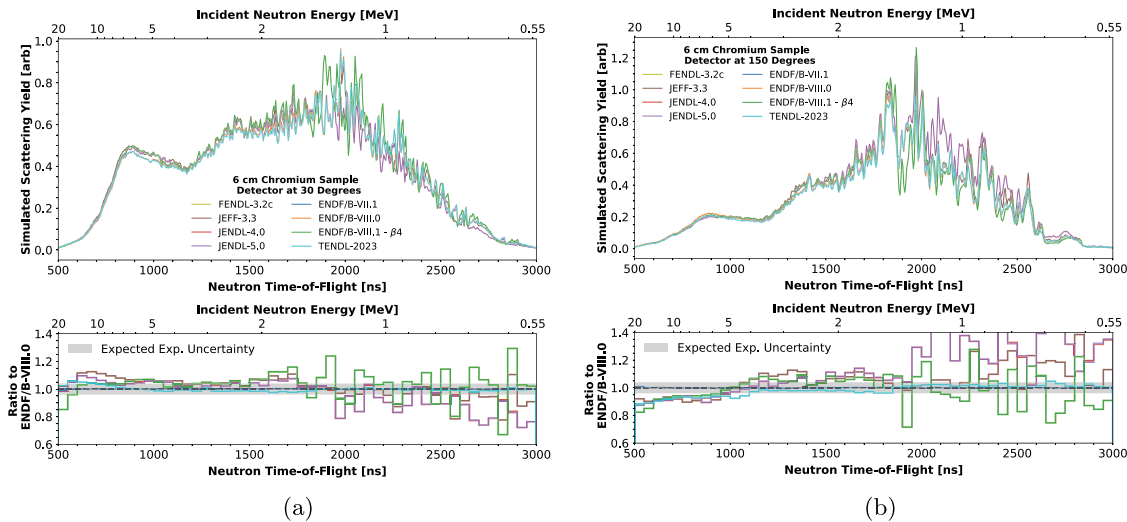


Fig. A.7. Expected computational results of several evaluated nuclear data libraries corresponding to a QD neutron scattering measurement of chromium at RPI.

neutron scattering yields calculated using several cobalt evaluated nuclear datasets are observed in Fig. A.8 with a peak difference of over 30% at 5 MeV at backward neutron scattering angles.

A.IX. FLiBe

FLiBe salt is a breeder material for nuclear fusion reactor concepts (Table I). Discrepancies of up to 50% in the simulated neutron scattering yields of FLiBe using different evaluated nuclear data are observed below 2 MeV at both forward and backward neutron scattering

angles. Nuclear data for all FLiBe constituents were varied, and sample containment was not considered for this calculation.

A.X. HAFNIUM

Hafnium is candidate high-Z material for plasma facing materials and shielding in nuclear fusion reactors (Table I). It is also a strong absorber of thermal neutrons. The different evaluated Hf nuclear datasets used in this calculation predict neutron scattering yields which disagree by up to 40% and 50% below 10 MeV at both

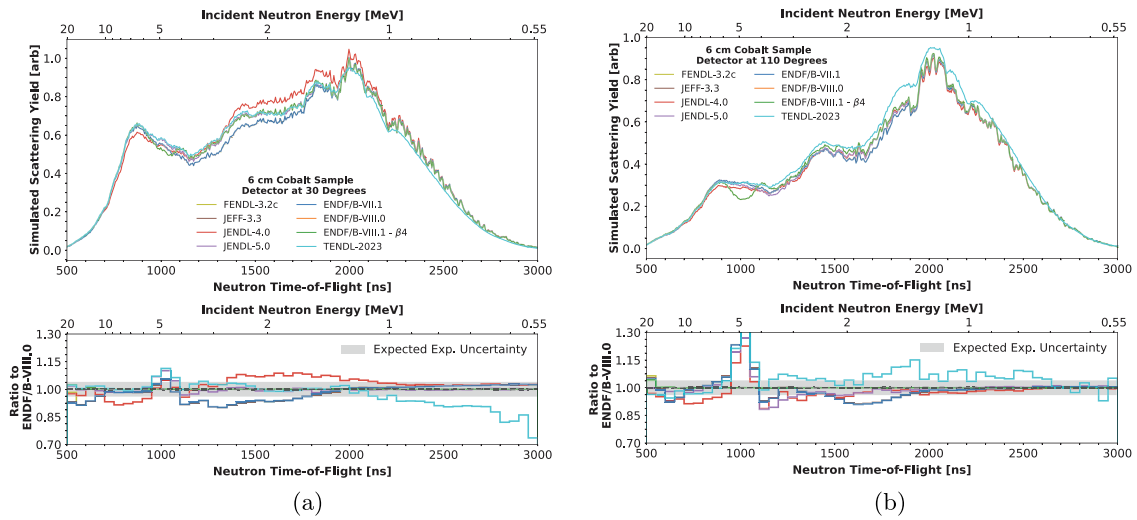


Fig. A.8. Expected computational results of several evaluated nuclear data libraries corresponding to a QD neutron scattering measurement of cobalt at RPI.

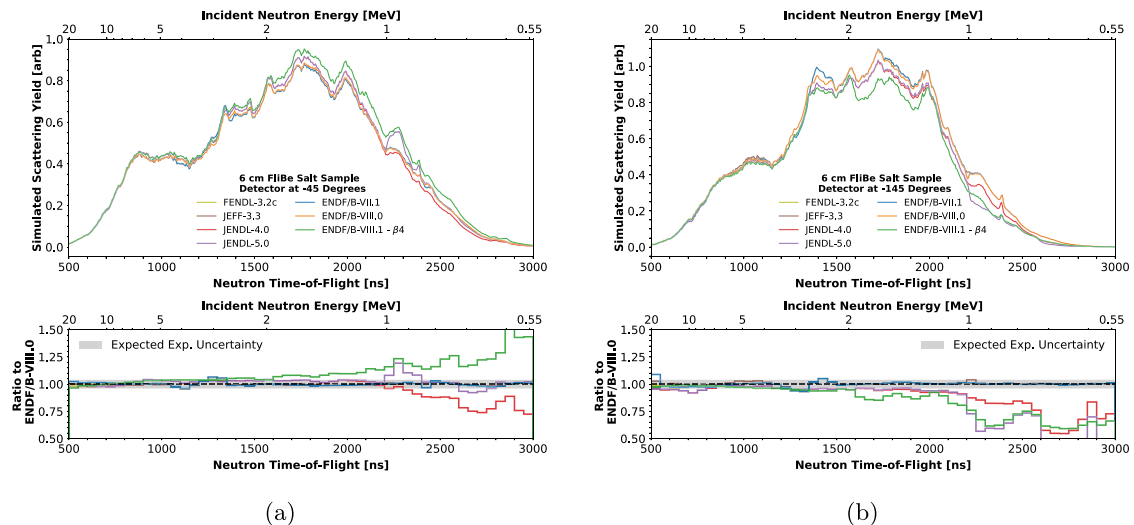


Fig. A.9. Expected computational results of several evaluated nuclear data libraries corresponding to a QD neutron scattering measurement of a FLiBe salt at RPI.

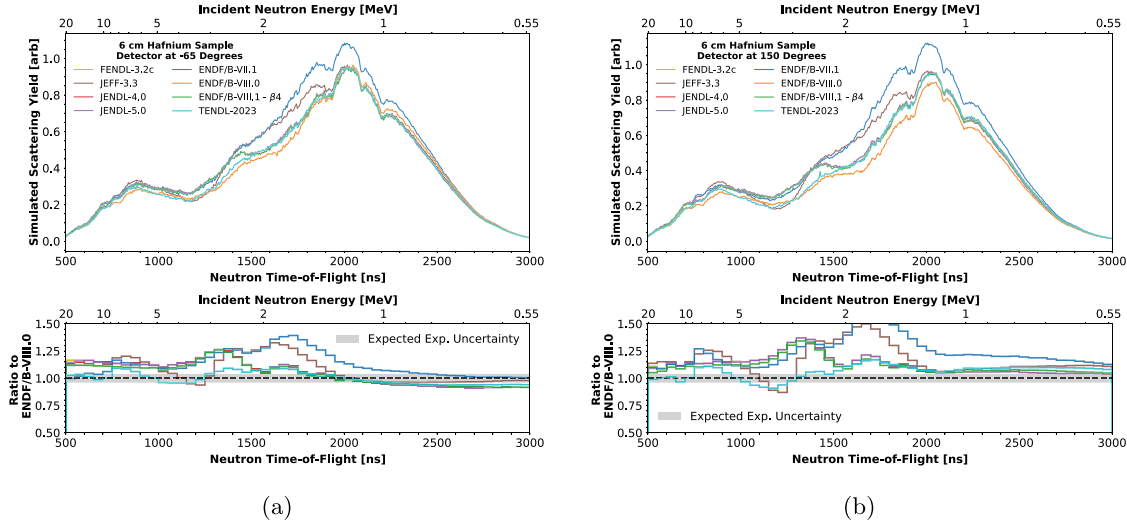


Fig. A.10. Expected computational results of several evaluated nuclear data libraries corresponding to a QD neutron scattering measurement of hafnium at RPI.

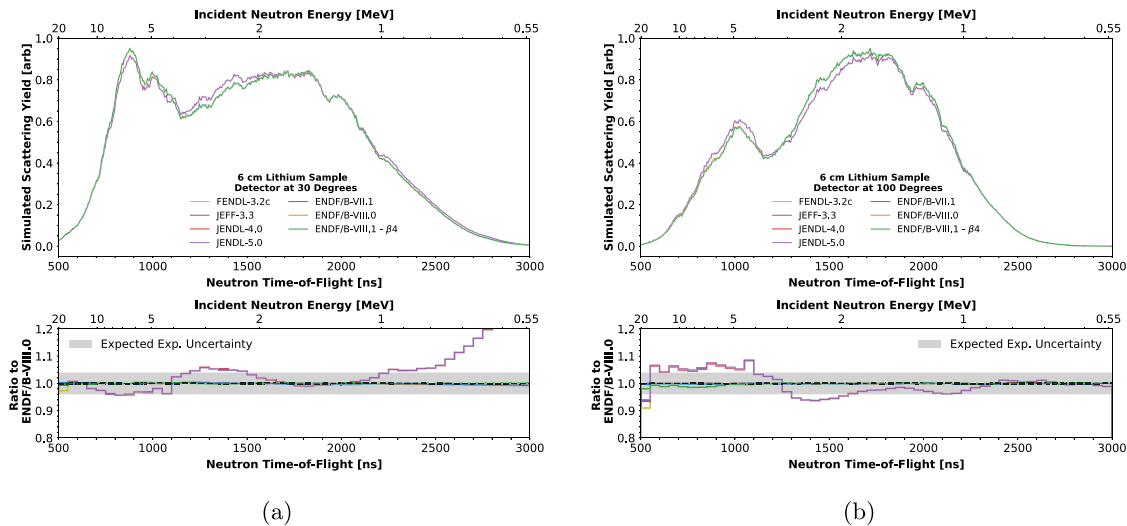


Fig. A.11. Expected computational results of several evaluated nuclear data libraries corresponding to a QD neutron scattering measurement of lithium at RPI.

forward and backward neutron scattering angles, respectively.

A.XI. LITHIUM

Most tritium breeder concepts in nuclear fusion reactors leverage lithium due to the high ${}^6\text{Li}(n,t)$ and ${}^7\text{Li}(n,Xt)$ cross sections. Neutron scattering yield calculations using evaluated lithium nuclear data from different nuclear data libraries are approximately 10% discrepant above 5 MeV at backward neutron scattering angles. At forward neutron scattering angles, a 20% discrepancy is also observed below 1

MeV. Sample containment was not considered for the calculation.

A.XII. MAGNESIUM

Magnesium, in the form of magnesium oxide (MgO) or magnesium aluminate (MgAl_2O_4), can be used as an insulating material for electrical components in a nuclear fusion device (Table I). Magnesium is also present in concrete. In Figure A.12, it is observed that all Mg nuclear data evaluations considered, except for those of TENDL-2023, are mostly the same. Due to its lack of resonance structure, the TENDL-2023 evaluation is up to

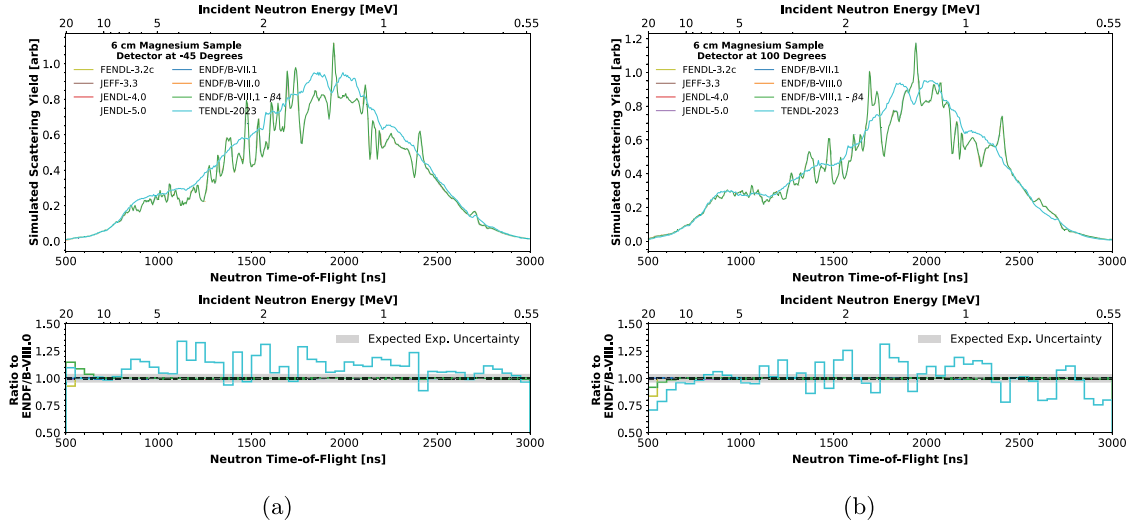


Fig. A.12. Expected computational results corresponding to a QD neutron scattering measurement of magnesium at RPI.

40% discrepant with other evaluations throughout the entire experimental energy region (~ 0.5 MeV to 20 MeV). Sample containment was not considered for the calculation.

A.XIII. MANGANESE

Manganese is an essential component of most steels, some of which are considered for structural use in nuclear fusion systems (Table I). In Fig. A.13, resonance structure is observable in the neutron scattering yields predicted by some evaluated manganese nuclear datasets investigated. Differences in manganese neutron scattering cross section representations by different evaluations lead to inconsistencies of up to 35% between their respective

simulated neutron scattering yields below 5 MeV at both forward and backward neutron scattering angles.

A.XIV. POTASSIUM

Potassium is a primary constituent of the FLiNaK tritium breeding concept (Table I), and it is present in concrete. The simulated neutron scattering yields between the different evaluated potassium datasets considered in this analysis vary significantly (over 60%), particularly below 1.5 MeV and above 10 MeV. Furthermore, an unusually rapid change in the scattering yield is observed at around 1.5 MeV in the JEFF-3.3 and FENDL-3.2c evaluations which is not present in the other libraries

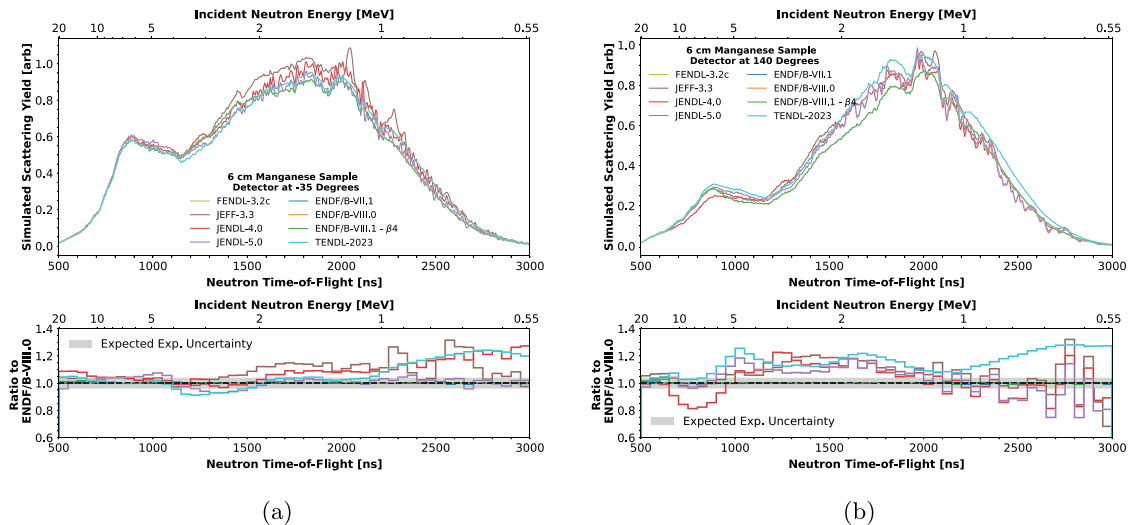


Fig. A.13. Expected computational results corresponding to a QD neutron scattering measurement of manganese at RPI.

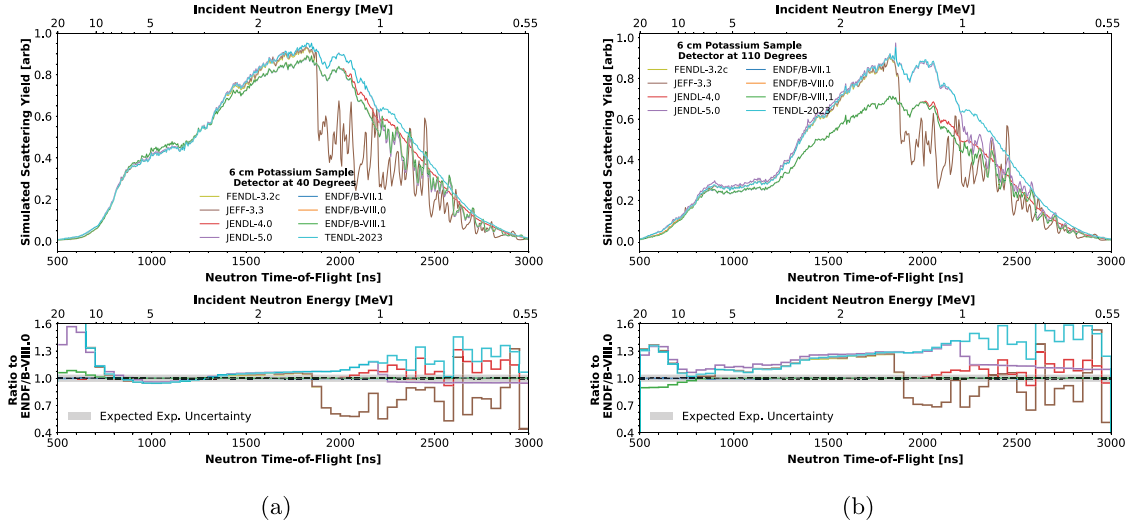


Fig. A.14. Expected computational results corresponding to a QD neutron scattering measurement of potassium at RPI.

tested. Sample containment was not considered for this calculation.

A.XV. SODIUM

Sodium is a primary constituent of both the FLiNaBe and FLiNaK tritium breeding concepts (Table I), and it is present in concrete. To emulate a realistic experiment, sodium chloride (NaCl) was modeled. In Fig. A.15 it is observed that the different sodium evaluated nuclear datasets considered in this analysis disagree by up to 40% below 2 MeV at both forward and backward neutron scattering angles due to differences in neutron resonance representation. Only sodium nuclear data was varied in

these simulations, and sample containment was not considered.

A.XVI. SULFUR

Sulfur is used as an alloying material for high strength steels which may be used in the construction of nuclear fusion systems, and it is present in concrete (Table I). In Fig. A.16 the neutron scattering yields calculated using different sulfur evaluated nuclear data are observed to disagree by up to 60% in the region of sharp resonances between 1 and 2 MeV at both forward and backward neutron scattering angles. Sample containment was not considered for this calculation.

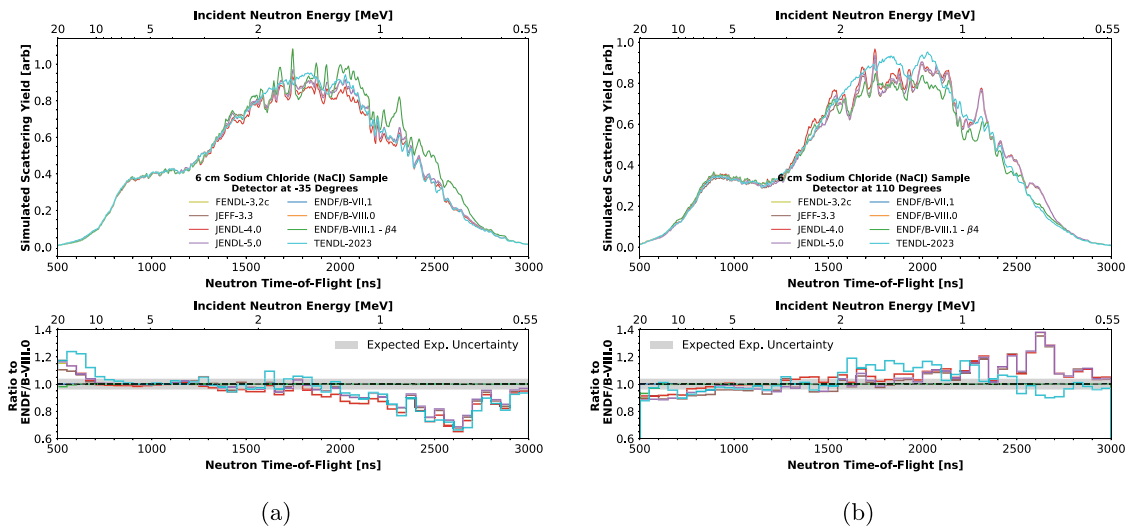


Fig. A.15. Expected computational results corresponding to a QD neutron scattering measurement of sodium chloride at RPI; varying sodium nuclear data only.

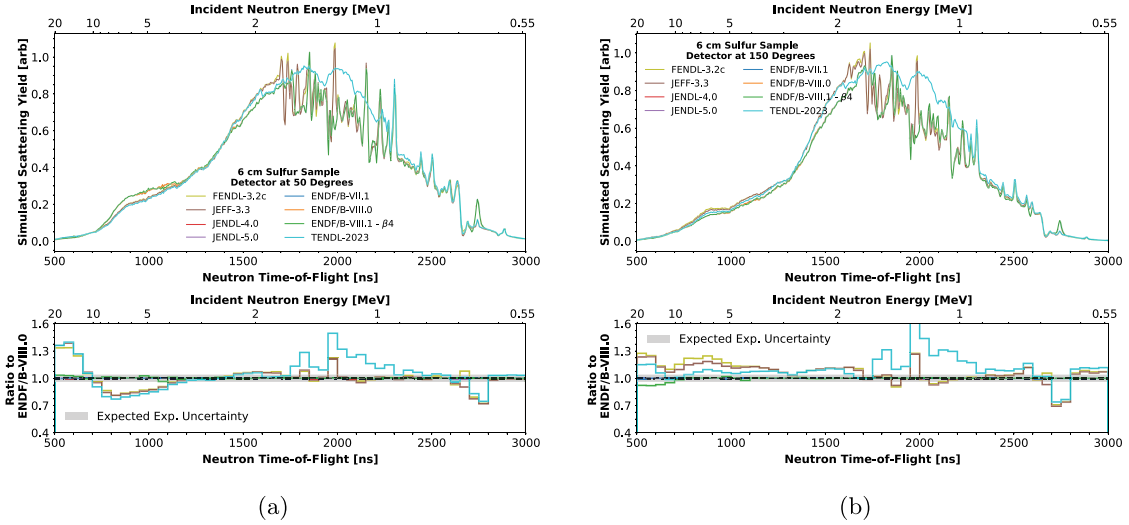


Fig. A.16. Expected computational results of several evaluated nuclear data libraries corresponding to a QD neutron scattering measurement of sulfur at RPI.

A.XVII. NITROGEN

Nitrogen is a common activation product in nuclear fusion systems, and it can also be used in insulating compounds. In effort to emulate a realistic experiment and maximize nitrogen atomic density, a sample of ammonia (NH_3) was modeled. The simulated neutron scattering yields of ammonia using different nitrogen evaluated nuclear data disagree by up to 30% in the region of large nitrogen resonances between 2 and 7 MeV at both forward and backward neutron scattering angles. Sample containment was not considered for this calculation.

A.XVIII. NICKEL

Nickel is a common element used in the fabrication of most steels which are considered for use in nuclear fusion reactors (Table I). Strong neutron resonance structure in nickel is visible below 3 MeV in the simulated neutron scattering yields shown in Fig. A.18. Inconsistencies in the representation of these resonances between the evaluated nuclear datasets considered lead to observed differences of up to 20% at both forward and backward neutron scattering angles. Additional disagreements of up to 20% are visible above 10 MeV.

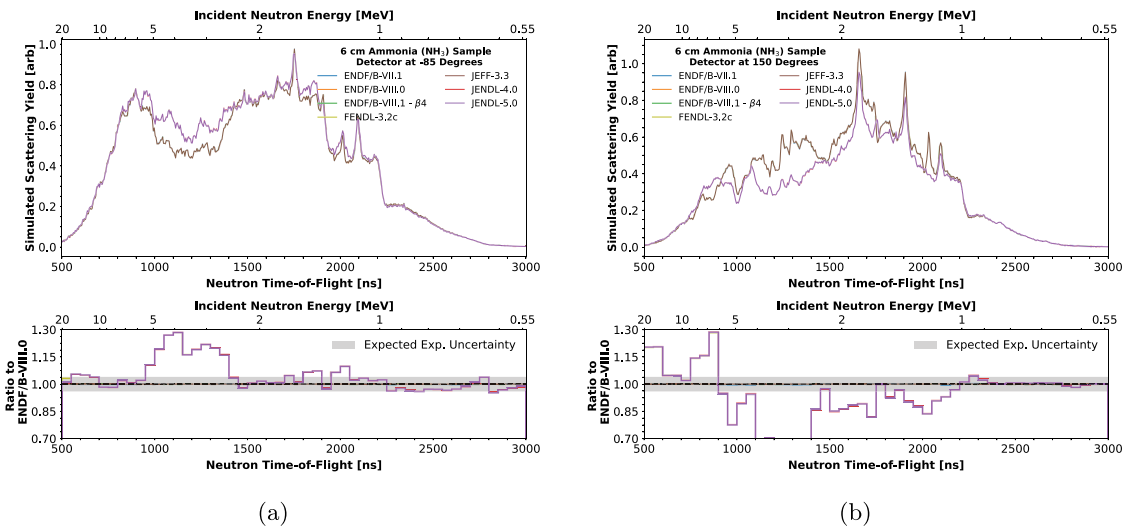


Fig. A.17. Expected computational results corresponding to a QD neutron scattering measurement of ammonia at RPI; varying nitrogen nuclear data only.

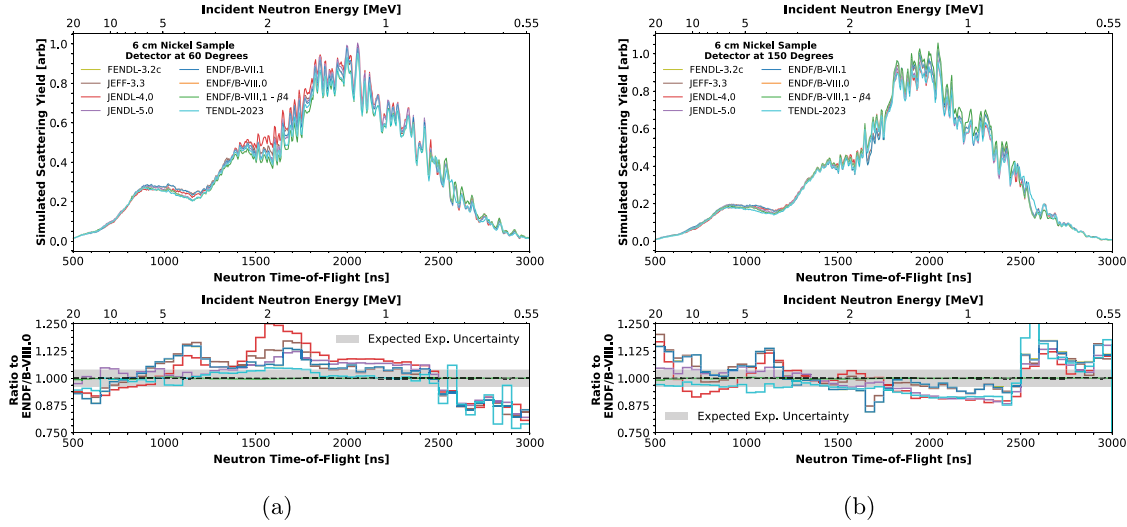


Fig. A.18. Expected computational results corresponding to a QD neutron scattering measurement of nickel at RPI.

A.XIX. TIN

Tin is a primary constituent of Nb_3Sn super-conducting magnets which are a leading candidate for use in magnetic confinement nuclear fusion reactors (Table I). The neutron scattering yields from tin calculated using different evaluated nuclear data are provided in Fig. A.19, where disagreements of up to 20% are observed both forward and backward neutron scattering angles above 2 MeV.

A.XX. YTTRIUM

Yttrium is a key element used in yttrium barium copper oxide (YBCO) super conductors, which are under development for use in nuclear fusion reactors (Table I). In Fig. A.20 it is observed that the simulated neutron scattering yields calculated using different yttrium evaluated nuclear data differ by up to 25% at both forward and backward neutron scattering angles below 10 MeV. Sample containment was not considered for this calculation.

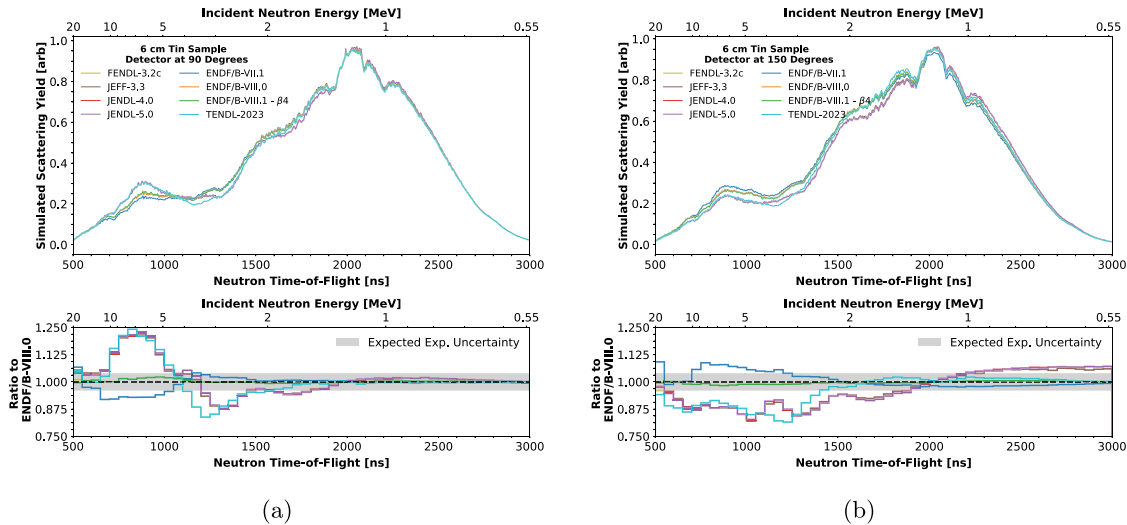


Fig. A.19. Expected computational results corresponding to a QD neutron scattering measurement of tin at RPI.

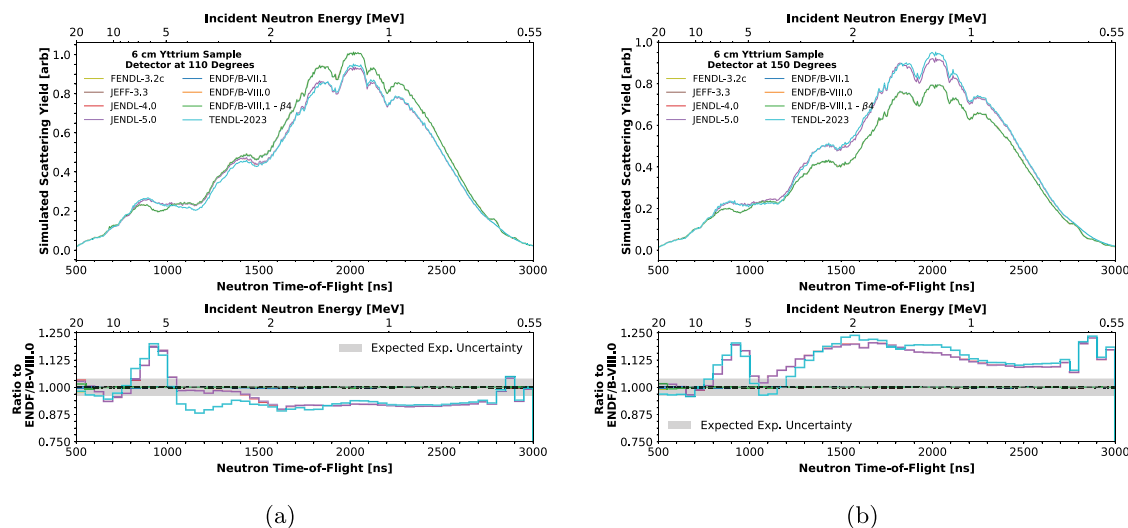


Fig. A.20. Expected computational results corresponding to a QD neutron scattering measurement of yttrium at RPI.

Disclosure Statement

No potential conflict of interest was reported by the author(s).



Author contributions

CRedit: **Gregory Siemers:** Data curation, Formal analysis, Investigation, Writing – original draft; **Yaron Danon:** Conceptualization, Investigation, Funding acquisition, Supervision, Writing – review & editing.

Funding

The authors thank the Nuclear Criticality Safety Program, funded and managed by the National Nuclear Security Administration for the U.S. Department of Energy, for sponsoring part of this work. One of the authors (Siemers) was supported in part by both the U.S. Nuclear Regulatory Commission [grant NRC-HQ-60-17-G-0006] and the U.S. National Nuclear Security Administration office of Naval Reactors' Naval Nuclear Propulsion Program.

ORCID

Gregory Siemers  <http://orcid.org/0000-0002-7664-2208>
Yaron Danon  <http://orcid.org/0000-0001-6187-9731>

References

1. M. A. LIVELY, et al. "Calculations of Radiation Back-Flux from Neutron Irradiation in Fusion Reactors,"

LA- UR-24-28542, Rev. 1, Los Alamos National Laboratory (2024); <https://www.osti.gov/biblio/2447586> (current as of June 19, 2025).

2. D. ROCHMAN, A. KONING, and S. van der MARCK, "Exact Nuclear Data Uncertainty Propagation for Fusion Neutronics Calculations," *Fusion Eng. Des.*, **85**, 5, 669 (2010); <https://doi.org/10.1016/j.fusengdes.2010.03.034>.
3. N.-G. TOKAI-MURA and IBARAKI-KEN, "Collection of Experimental Data for Fusion Neutronics Benchmark," JAERI-M 94-014, Japan Atomic Energy Research Institute (1994).
4. A. MILOCCO, A. TRKOV, and I. A. KODELI, "The OKTAVIAN TOF Experiments in SIN- BAD: Evaluation of the Experimental Uncertainties," *Ann. Nucl. Energy*, **37**, 4, 443 (2010); <https://doi.org/10.1016/j.anucene.2009.12.016>.
5. D. NEUDECKER et al., "Which Nuclear Data Can Be Validated with LLNL Pulsed-Sphere Experiments?," *Ann. Nucl. Energy*, **159**, 108345 (2021); <https://doi.org/10.1016/j.anucene.2021.108345>.
6. D. LAGHI et al., "JADE, a New Software Tool for Nuclear Fusion Data Libraries Verification & Validation," *Fusion Eng. Des.*, **161**, 112075 (2020); <https://doi.org/10.1016/j.fusengdes.2020.112075>.
7. D. LAGHI et al., "Application of JADE V and V Capabilities to the New FENDL v3.2 Beta Release," *Nucl. Fusion*, **61**, 11, 116073 (2021); <https://doi.org/10.1088/1741-4326/ac121a>.
8. A. J. M. PLOMPEN et al., "The Joint Evaluated Fission and Fusion Nuclear Data Library, JEFF-3.3," *Eur. Phys. J. A*, **56**, 181 (2020).

9. O. IWAMOTO et al., “Japanese Evaluated Nuclear Data Library Version 5: JENDL-5,” *J. Nucl. Sci. Technol.*, **60**, 1 (2023); <https://doi.org/10.1080/00223131.2022.2141903>.
10. D. BROWN et al., “ENDF/B-VIII.0: The 8th Major Release of the Nuclear Reaction Data Library with CIELO-Project Cross Sections, New Standards and Thermal Scattering Data,” *Nucl. Data Sheets*, **148**, 1 (2018); <https://doi.org/10.1016/j.nds.2018.02.001>.
11. B. EBIWONJUMI and E. PETERSON, “Uncertainty Analyses of Tritium Production and Gamma Heating Rates in the FNS Clean Benchmark Experiments,” SSRN (2024) <https://doi.org/10.2139/ssrn.4949078>.
12. B. KOS et al., “Nuclear Data Uncertainty Propagation in Complex Fusion Geometries,” *J. Nucl. Eng.*, **1**, 1, 63 (2020); <https://doi.org/10.3390/jne1010006>.
13. G. SCHNABEL et al., “FENDL: A Library for Fusion Research and Applications,” *Nucl. Data Sheets*, **193**, 1 (2024); <https://doi.org/10.1016/j.nds.2024.01.001>.
14. M. SAWAN, “FENDL Neutronics Benchmark: Specifications for the Computational and Shielding Benchmark,” INDC(NDS)-316, International Atomic Energy Agency (1994).
15. G. NOBRE et al., “ENDF/B-VIII.1: Updated Nuclear Reaction Data Library for Science and Applications,” *Nuclear Data Sheets* (To be Published).
16. D. LOPEZ ALDAMA and A. TRKOV, “FENDL-2.1: Update of an Evaluated Nuclear Data Library for Fusion a Applications,” International Atomic Energy Agency, (Dec. 2004); <https://www-nds.iaea.org/publications/indc/indc-nds-0467/>.
17. R. FORREST et al., “FENDL-3 Library Summary Documentation,” International Atomic Energy Agency, (Dec. 2012); <https://doi.org/10.61092/iaea.me5j-xqk3>.
18. A. RAFFRAY et al., “Breeding Blanket Concepts for Fusion and Materials Requirements,” *J. Nucl. Mater.*, **307–311**, 21 (2002); [https://doi.org/10.1016/S0022-3115\(02\)01174-1](https://doi.org/10.1016/S0022-3115(02)01174-1).
19. T. TANABE, *Characteristics of Tritium*, pp. 27–48, Springer Japan, Tokyo (2016).
20. A. CARLSON et al., “Evaluation of the Neutron Data Standards,” *Nucl. Data Sheets*, **148**, 143 (2018); <https://doi.org/10.1016/j.nds.2018.02.002>.
21. F. J. SAGLIME, “High Energy Nuclear Differential Scattering Measurements for Beryllium and Molybdenum,” PhD Thesis, Rensselaer Polytechnic Institute (2009).
22. F. SAGLIME et al., “A System for Differential Neutron Scattering Experiments in the Energy Range from 0.5 to 20 MeV,” *Nucl. Instrum. Methods Phys. Res. Sect. A*, **620**, 2–3, 401 (2010); <https://doi.org/10.1016/j.nima.2010.04.051>.
23. D. P. BARRY et al., “Quasi-Differential Neutron Scattering in Zirconium from 0.5 to 20 MeV,” *Nucl. Sci. Eng.*, **172**, 2, 188 (2013); http://www.ans.org/pubs/journals/nse/a_16857.
24. A. DASKALAKIS et al., “Quasi-Differential Elastic and Inelastic Neutron Scattering from Iron in the MeV Energy Range,” *Ann. Nucl. Energy*, **110**, 603 (2017); <https://doi.org/10.1016/j.anucene.2017.07.007>.
25. E. BLAIN et al., “Measurements of Neutron Scattering from a Copper Sample Using a Quasi-Differential Method in the Region from 2 keV to 20 MeV,” *Nucl. Sci. Eng.*, **196**, 2, 121 (2022); <https://doi.org/10.1080/00295639.2021.1961542>.
26. A. DASKALAKIS et al., “Quasi-Differential Neutron Scattering from ^{238}U from 0.5 to 20 MeV,” *Ann. Nucl. Energy*, **73**, 455 (2014); <https://doi.org/10.1016/j.anucene.2014.07.023>.
27. K. S. MOHINDROO et al., “Quasi- Differential Neutron Induced Neutron Emissions from ^{235}U , and ^{239}Pu ,” *Ann. Nucl. Energy*, **165**, 108647 (2022); <https://doi.org/10.1016/j.anucene.2021.108647>.
28. M. E. OVERBERG et al., “Photoneutron Target Development for the RPI Linear Accelerator,” *Nucl. Instrum. Methods Phys. Res. Sect. A*, **438**, 2, 253 (1999); [https://doi.org/10.1016/S0168-9002\(99\)00878-5](https://doi.org/10.1016/S0168-9002(99)00878-5).
29. A. M. DASKALAKIS, “Measurement of Elastic and Inelastic Neutron Scattering in the Energy Range from 0.5 to 20 MeV,” PhD Thesis, Rensselaer Polytechnic Institute (2015).
30. A. DASKALAKIS et al., “Examining and Modeling Gamma Emission from Quasi-Differential High Energy Scattering Measurements,” presented at the Workshop on Elastic and Inelastic Neutron Scattering (2023); https://indico.global/event/1304/contributions/27302/attachments/13808/21038/WINS_Presentation_2_Daskalakis.pdf (current as of June 19, 2025).
31. G. F. KNOLL, *Radiation Detection and Measurement*, John Wiley & Sons, Inc (2010).
32. R. LANG et al., “Improved Pulse Shape Discrimination in EJ-301 Liquid Scintillators,” *Nucl. Instrum. Methods Phys. Res. Sect. A*, **856**, 26 (2017); <https://doi.org/10.1016/j.nima.2017.02.090>.
33. J. K. DICKENS, “SCINFUL: A Monte Carlo Based Computer Program to Determine a Scintillator Full Energy Response to Neutron Detection for Energies Between 0.1 and 80 MeV: Program Development and Comparisons of Program Predictions with Experimental Data,” ORNL- 6463, Oak Ridge National Laboratory (1998).
34. M. E. RISING et al., “MCNP Code Version 6.3.0 Release Notes,” LA-UR-22-33103, Rev. 1, Los Alamos National Laboratory (2023); <https://doi.org/10.2172/1909545>.

35. G. SIEMERS et al., “A Quasi-Differential Measurement of Neutron Scattering from Tantalum Between 0.65 MeV and 20 MeV,” *Ann. Nucl. Energy*, **224**, 111676 (2025); <https://doi.org/10.1016/j.anucene.2025.111676>.
36. K. J. KELLY et al., “Measurement of the Cross Section of the $Q = 4.4398$ MeV $^{12}\text{C}(n, n'\gamma)$ Reaction from Threshold to 16.5 MeV Using γ and Correlated n - γ Detection,” *Phys. Rev. C*, **108**, 014603 (2023); <https://doi.org/10.1103/PhysRevC.108.014603>.
37. G. GKATIS et al., “Angular Distribution Measurements of Neutron Elastic Scattering on Natural Carbon,” *Phys. Rev. C*, **110**, 3, 034609 (2024); <https://doi.org/10.1103/PhysRevC.110.034609>.
38. T. IHLE et al., “Review of Blanket Designs for Advanced Fusion Reactors,” *Fusion Eng. Des.*, **83**, 7, 912 (2008); <https://doi.org/10.1016/j.fusengdes.2008.07.039>.
39. P. BRAIN et al., “Resolved Resonance Region Evaluations of $\text{N} + {}^{206,207,208}\text{Pb}$ for Fast Spectrum Applications,” *Ann. Nucl. Energy*, **202**, 110452 (2024); <https://doi.org/10.1016/j.anucene.2024.110452>.
40. P. BRAIN, “Neutron Evaluation and Validation of Natural Lead Isotopes for Fast Spectrum Systems,” PhD Thesis, Rensselaer Polytechnic Institute (2023).
41. A. E. YOUNG et al., “Fast Neutron Scattering Measurements with Lead,” presented at AccApp 15 (2015).
42. M. CHADWICK et al., “ENDF/B-VII.1 Nuclear Data for Science and Technology: Cross Sections, Covariances, Fission Product Yields and Decay Data,” *Nucl. Data Sheets*, **112**, 12, 2887 (2011); <https://doi.org/10.1016/j.nds.2011.11.002>.
43. K. SHIBATA et al., “JENDL-4.0: A New Library for Nuclear Science and Engineering,” *J. Nucl. Sci. Technol.*, **48**, 1 (2011); <https://doi.org/10.1080/18811248.2011.9711675>.
44. A. KONING et al., “TENDL: Complete Nuclear Data Library for Innovative Nuclear Science and Technology,” *Nucl. Data Sheets*, **155**, 1 (2019); <https://doi.org/10.1016/j.nds.2019.01.002>.
45. S. J. ZINKLE, “Advanced Materials for Fusion Technology,” *Fusion Eng. Des.*, **74**, 1, 31 (2005); <https://doi.org/10.1016/j.fusengdes.2005.08.008>.
46. S. SATO et al., “Progress in the Blanket Neutronics Experiments at JAERI/FNS,” *Fusion Eng. Des.*, **81**, 8, 1183 (2006); <https://doi.org/10.1016/j.fusengdes.2005.09.078>.
47. C. G. WINDSOR et al., “Tungsten Boride Shields in a Spherical Tokamak Fusion Power Plant,” *Nucl. Fusion*, **61**, 8, 086018 (2021); <https://doi.org/10.1088/1741-4326/ac09ce>.
48. B. KHRIPUNOV et al., “Study of Tungsten as a Plasma-Facing Material for a Fusion Reactor,” *Physics Procedia*, **71**, 63 (2015); <https://doi.org/10.1016/j.phpro.2015.08.313>.
49. Y. IKEDA et al., “Neutronics Experiment and Analysis on a Tungsten Slab Assembly Bombarded with D-T Neutrons,” *Fusion Eng. Des.*, **18**, 309 (1991); [https://doi.org/10.1016/0920-3796\(91\)90144-F](https://doi.org/10.1016/0920-3796(91)90144-F).
50. K. OKUNO, A. SHIKOV, and N. KOIZUMI, “Superconducting Magnet System in a Fusion Reactor,” *J. Nucl. Mater.*, **329–333**, 141 (2004); <https://doi.org/10.1016/j.jnucmat.2004.04.151>.
51. A. MOLODYK et al., “Development and Large Volume Production of Extremely High Current Density $\text{YBa}_2\text{Cu}_3\text{O}_7$ Superconducting Wires for Fusion,” *Sci. Rep.*, **11**, 1, 2084 (2021); <https://doi.org/10.1038/s41598-021-81559-z>.
52. T. MUROGA et al., “Present Status of Vanadium Alloys for Fusion Applications,” *J. Nucl. Mater.*, **455**, 1, 263 (2014); <https://doi.org/10.1016/j.jnucmat.2014.06.025>.
53. S. NISHIO, “Conceptual Design of Advanced Steady-State Tokamak Reactor (A-SSTR2) – Compact and Safety Oriented Commercial Power Plant. Proc.18th IAEA Fusion Energy Conf. (IAEA-CSP-8/C; IAEA-CN-77; FTP-2/14), IAEA (2001).
54. F. HERNANDEZ et al. “A New HCPB Breeding Blanket for the EU DEMO: Evolution, Rationale and Preliminary Performances,” *Fusion Eng. Des.*, **124**, 882 (2017); <https://doi.org/10.1016/j.fusengdes.2017.02.008>.
55. L. M., GIANCARLI et al., “Overview of the ITER TBM Program,” *Fusion Eng. Des.*, **8**, 395 (2012); <https://doi.org/10.1016/J.FUSENGDES.2011.11.005>.
56. L. M., GIANCARLI et al., “Status of the ITER TBM Program and Overview of its Technical Objectives,” *Fusion Eng. Des.*, **203**, 114424 (2024); <https://doi.org/10.1016/j.fusengdes.2024.114424>.
57. L. GIANCARLI et al. “Development of the EU Water-Cooled Pb-17Li Blanket,” *Fusion Eng. Des.*, **39–40**, 639 (1998); [https://doi.org/10.1016/S0920-3796\(97\)00138-5](https://doi.org/10.1016/S0920-3796(97)00138-5).
58. M. ZAUPA et al., “Balance of Plant Conceptual Design of EU DEMO Integrating Different Breeding Blanket Concepts,” *Fusion Eng. Des.*, **200**, 114235 (2024); <https://doi.org/10.1016/j.fusengdes.2024.114235>.
59. M. GASPAROTTO et al., “Demo Blanket Technology R and D Results in EU,” *Fusion Eng. Des.* **61–62**, 263 (2002); [https://doi.org/10.1016/S0920-3796\(02\)00170-9](https://doi.org/10.1016/S0920-3796(02)00170-9).
60. B. GARCINUÑO et al., “Establishing Technical Specifications for PbLi Eutectic Alloy Analysis and its Relevance in Fusion Applications,” *Nucl. Mater. Energy*, **300**, 101146 (2022); <https://doi.org/10.1016/j.nme.2022.101146>.
61. S. MALANG et al., “Development of Self-Cooled Liquid Metal Breeder Blankets,” (Nov. 1995).
62. F. NAJMABADI et al. “The ARIES-AT Advanced Tokamak, Advanced Technology Fusion Power Plant,”

- Fusion Eng. Des.*, **80**, 3 (2006); <https://doi.org/10.1016/j.fusengdes.2005.11.003>
63. F. NAJMABADI et al., “The ARIES-I Tokamak Reactor Study, Final Report,” UCLA-PPG-1323, UCLA (1991).
 64. S. SHARAFAT et al., “ARIES-I Fusion-Power-Core Engineering,” *Fusion Eng. Des.*, **18**, 215 (1991), [https://doi.org/10.1016/0920-3796\(91\)90130-I](https://doi.org/10.1016/0920-3796(91)90130-I)
 65. M. S. TILLACK and ARIES Team, “Engineering Design of the ARIES-RS Power Plant,” *Fusion Eng. Des.*, **41**, 491 (1998); [https://doi.org/10.1016/S0920-3796\(97\)00161-0](https://doi.org/10.1016/S0920-3796(97)00161-0)
 66. R. MATTAS et al., Evaporation Cooling Concept, EVOLVE APEX Interim Report. <https://bpb-us-w2.wpmucdn.com/research.seas.ucla.edu/dist/d/39/files/2019/08/chapter10full1.pdf>
 67. R. F. MATTAS et al., “EVOLVE—An Advanced First Wall/Blanket System,” *Fusion Eng. Des.*, **49–50**, 613 (2000); [https://doi.org/10.1016/S0920-3796\(00\)00350-1](https://doi.org/10.1016/S0920-3796(00)00350-1)
 68. B. PINT et al., “Materials Assessment for FLiBe Fusion Blankets,” Oak Ridge National Laboratory (2024); <https://www.osti.gov/biblio/2455087> (current as of June 19, 2025).
 69. S. FUKADA et al., “Our Recent Experimental Challenges on FLiBe or FLiNaBe Coolant for Fusion Applications and Related Japanese Research,” IAEA TecDoc 1912, Kyushu University (2017).
 70. E. T. CHENG et al. “Nuclear aspects of molten salt blankets,” *Fusion Eng. Des.*, **69**, (2003) 205-213; [https://doi.org/10.1016/S0920-3796\(03\)00339-9](https://doi.org/10.1016/S0920-3796(03)00339-9)
 71. T. TANAKA et al. “Liquid Blanket Collaboration Platform Oroshhi-2 at NIFS with FLiNaK/LiPb Twin Loops,” *Fusion Sci. Technol.*, **75**, 1002 (2019); <https://doi.org/10.1080/15361055.2019.1658044>
 72. N. E. GOTH et al. “Optimal Chloride Saly Mixture for a Fusion Blanket” ORNL/TM-2023/3052 (Sept. 2023); <https://info.ornl.gov/sites/publications/Files/Pub201058.pdf>
 73. U. FISCHER et al., “Neutronics and Nuclear Data: Achievements in Computational Simulations and Experiments in Support of Fusion Reactor Design,” *Fusion Eng. Des.*, **51–52**, 663 (2000); [https://doi.org/10.1016/S0920-3796\(00\)00236-2](https://doi.org/10.1016/S0920-3796(00)00236-2).
 74. Y. ZHAI et al., “Conceptual Magnet Design Study for Fusion Nuclear Science Facility,” *Fusion Eng. Des.*, **135**, 324 (2018); <https://doi.org/10.1016/j.fusengdes.2017.06.028>.
 75. M. ABDOU, “Radiation Considerations for Superconducting Fusion Magnets,” *J. Nucl. Mater.*, **72**, 1, 147 (1978); [https://doi.org/10.1016/0022-3115\(78\)90398-7](https://doi.org/10.1016/0022-3115(78)90398-7).
 76. N. MITCHELL et al. “The ITER Magnets: Design and Construction Status,” *IEEE Trans. Appl. Supercond.*, **22**, 4200809 (June 2012); <https://doi.org/10.1109/TASC.2011.2174560>.
 77. T. KELHAR, “SPARC-Experimental Fusion Device.” <https://matrika.fmf.uni-lj.si/letnik-8/stevilka-2/kelhar.pdf>
 78. Z. S. HARTWIG et al., “The SPARC Toroidal Field Model Coil Program,” *IEEE Trans. Appl. Supercond.*, **34**, 0600316 (Mar. 2024); <https://doi.org/10.1109/TASC.2023.3332613>.
 79. S. ZINKLE et al., “Scientific and Engineering Advances from Fusion Materials R&D,” *J. Nucl. Mater.*, **307–311**, 31 (2002); [https://doi.org/10.1016/S0022-3115\(02\)01088-7](https://doi.org/10.1016/S0022-3115(02)01088-7).
 80. R. BEHRISCH, “Plasma-Facing Materials for Fusion Devices,” *J. Surf. Invest.: X-ray, Synchrotron and Neutron Tech.*, **4**, 4, 549 (2010); <https://doi.org/10.1134/S1027451010040014>.
 81. A. HASEGAWA et al., “Neutorn Irradiation Behavior of Tungsten,” *Mater. Trans.*, **54**, 466 (2013); <https://doi.org/10.2320/matertrans.MG201208>
 82. S. A. HUMPHRY-BAKER, “Shielding Materials in the Compact Spherical Tokamak,” *Phil. Trans. R. Soc.*, **377**, 20170443 (2019); <http://doi.org/10.1098/rsta.2017.0443>
 83. S. AKBAS et al., “Neutron Shielding Calculation for DEMO-Prad/SXR Measurement System,” *Phys. Plasmas*, **31**, 033112 (2024); <https://doi.org/10.1063/5.0199683>
 84. J. BROOKS et al., “Plasma-Facing Material Alternatives to Tungsten,” *Nucl. Fusion*, **55**, 4, 043002 (2015); <https://doi.org/10.1088/0029-5515/55/4/043002>.
 85. E.E. BLOOM, “Structural Materials for Fusion Reactors,” *Nucl. Fusion*, **30**, 1879 (1990); <https://doi.org/10.1088/0029-5515/30/9/012>
 86. Z. OKSIUTA and N. BALUC, “Optimization of the Chemical Composition and Manufacturing Route for ODS RAF Steels for Fusion Reactor Application,” *Nucl. Fusion*, **49**, 055003 (2009); <https://doi.org/10.1088/0029-5515/49/5/055003>.
 87. M. ZMITKO et al. “The European ITER Test Blanket Modules: EUROFER97 Material and TBM’s Fabrication Technologies Development and Qualification,” *Fusion Eng. Des.*, **124**, 767 (2017); <https://doi.org/10.1016/j.fusengdes.2017.04.051>
 88. G. STORNELLI et al., “Ultra-Fine Grained EUROFER97 Steel for Nuclear Fusion Applications,” *J. Mater. Res. Technol.*, **33**, 5075 (2024); <https://doi.org/10.1016/j.jmrt.2024.10.069>.
 89. P. J. BARRON et al., “Towards V-Based High-Entropy Alloys for Nuclear Fusion Applications,” *Scr. Mater.*, **176**, 12–16 (2020); <https://doi.org/10.1016/j.scriptamat.2019.09.028>
 90. G. PIATTI, P. FIORINI, P. SCHILLER, “High Purity Aluminium Alloys for Experimental Fusion Reactors,” *Nucl. Eng. Des. Fusion*, **1**, 137 (1984); [https://doi.org/10.1016/0167-899X\(84\)90036-3](https://doi.org/10.1016/0167-899X(84)90036-3)
 91. B. A. BURGAN and S. BINGHAM, “An Innovative Form of Steel-Concrete (SC) Structures for Nuclear Power Plant,” Trans., SMIRT–24; BEXCO, Busan, Korea, August 20-25, 2017; <https://repository.lib.ncsu.edu/server/api/core/bitstreams/921ddbea-2e72-4283-a056-74f3ac5619c4/content>

92. J. J. CORDIER et al., “Overview of the ITER Tokamak Complex Building and Integration of Plant Systems Toward Construction,” *Fusion Eng. Des.*, **96–97**, 240 (2015); <https://doi.org/10.1016/j.fusengdes.2015.06.115>.
93. A. V. BEZNOSOV, S. S. PINAEV, and E. MURAV'EV, “Application of Lead and Lead-Bismuth in the Heat-Removal Systems of Tokamak Reactors,” *At. Energy*, **98**, 2, 103 (2005); <https://libproxy.rpi.edu/login?url=https://www.proquest.com/scholarly-journals/application-lead-bismuth-heat-removal-systems/docview/758905007/se-2> (current as of June 19, 2025).
94. “Insulators for Fusion Applications” IAEA-TECDOC-417, IAEA (Jun . 1986); https://inis.iaea.org/collection/NCLCollectionStore/_Public/18/077/18077885.pdf
95. A. DHABA'AN and T. BEYNON, “Three-Dimensional Analyses of Candidate Blanket Designs for the Compact Tokamak Reactor Concept,” *Prog. Nucl. Energy*, **29**, 1 (1995); <https://doi.org/10.1016/0149-19709400013-V>.
96. L. BOCCACCINI et al., “Advanced Helium Cooled Pebble Bed Blanket, Task PPA2.6, Final Report,” FZKA 6402, Forschungszentrum Karlsruhe (2000).
97. M. KIKUCHI et al., “Conceptual Design of the Steady State Tokamak Reactor (SSTR),” *Fusion Eng. Des.*, **18**, 195 (1991); [https://doi.org/10.1016/0920-3796\(91\)90127-C](https://doi.org/10.1016/0920-3796(91)90127-C)
98. M. KIKUCHI, “A Review of Fusion and Tokamak Research Towards Steady-State Operation: A JAEA Contribution,” *Energies*, **3**, 1741 (2010); <https://doi.org/10.3390/en3111741>